Title: Gene regulatory networks controlling differentiation, survival, and diversification of hypothalamic Lhx6-expressing GABAergic neurons.

Authors: Dong Won Kim[1], Kai Liu[1,10], Zoe Qianyi Wang[1], Yi Stephanie Zhang[1], Abhijith Bathini[1], Matthew P Brown[1], Sonia Hao Lin[1], Parris Whitney Washington[1], Changyu Sun[1], Susan Lindtner[7], Bora Lee[8], Hong Wang[1], Tomomi Shimogori[9], John L.R. Rubenstein[7], Seth Blackshaw[1-6]

Affiliations: [1]Solomon H. Snyder Department of Neuroscience, [2]Department of Ophthalmology, [3]Department of Neurology, [4]Center for Human Systems Biology, [5]Institute for Cell Engineering, [6]Kavli Neuroscience Discovery Institute, Johns Hopkins University School of Medicine, Baltimore, MD, 21205, USA, [7]Nina Ireland Laboratory of Developmental Neurobiology, Department of Psychiatry, UCSF Weill Institute for Neurosciences, University of California, San Francisco, San Francisco, CA 94158, USA, [8]Center for Neuroscience, Korea Institute of Science and Technology (KIST), Seoul, 02792, Korea, [9]RIKEN Center for Brain Science, Laboratory for Molecular Mechanisms of Brain Development, 2-1 Hirosawa, Wako, Saitama, 351-0198, Japan. [10]Present address: Genentech, South San Francisco, CA 94080.

Address all correspondence to sblack@jhmi.edu (S.B.)

Abstract:

GABAergic neurons of the hypothalamus regulate many innate behaviours, but little is known about the mechanisms that control their development. We previously identified hypothalamic neurons that express the LIM homeodomain transcription factor Lhx6, a master regulator of cortical interneuron development, as sleep-promoting. In contrast to telencephalic interneurons, hypothalamic Lhx6 neurons do not undergo long-distance tangential migration, and do not express cortical interneuronal markers such as *Pvalb*. Here, we show that *Lhx6* is necessary for survival of hypothalamic neurons, and that *Dlx1/2*, *Nkx2-2*, and *Nkx2-1* are each required for specification of spatially distinct subsets of hypothalamic Lhx6 neurons. We identify a broad range of neuropeptides that are enriched in spatially segregated subsets of hypothalamic Lhx6 neurons, and distinct from those seen in cortical neurons. These findings identify common and divergent mechanisms by which Lhx6 controls the development of GABAergic neurons in the hypothalamus compared to telencephalic interneurons.

Introduction:

Although much is now known about both the diversity and development of GABAergic neurons of the telencephalon (Huang and Paul, 2019; Lim et al., 2018), far less is known about their counterparts in the hypothalamus, where over 20% of neurons are GABAergic (Erö et al., 2018). Previous work shows that hypothalamic GABAergic neuronal precursors first appear in a domain that separates the anterodorsal and posteroventral halves of the developing hypothalamus, and is delineated by expression of transcription factors that regulate development of telencephalic GABAergic neurons, including *Dlx1/2* and *Arx* (Bedont et al., 2015; Bulfone et al., 1993; Cobos et al., 2005; Colasante et al., 2008; Shimogori et al., 2010). Within this structure, which has been termed the intrahypothalamic diagonal/tuberomamillary terminal (ID/TT), nested expression domains of LIM homeodomain family genes are observed, in which expression of *Lhx1*, *Lhx8*, and *Lhx6* delineates the anterior-posterior axis of the ID/TT (Shimogori et al., 2010). *Lhx1* is essential for terminal differentiation and function of neurons in the master circadian oscillator in the suprachiasmatic nucleus (Bedont et al., 2017, 2014; Hatori et al., 2014). Lhx6-expressing neurons in the zona incerta (ZI) of the hypothalamus are sleep-promoting and activated by elevated sleep pressure, and hypothalamic-specific loss of function of *Lhx6* disrupts sleep homeostasis (Liu et al., 2017).

Lhx6 has been extensively studied in the developing telencephalon. It is essential for the specification, migration and maturation of GABAergic neurons of the telencephalon – particularly the cortex and hippocampus (Kessaris et al., 2014; Maroof et al., 2010). Lhx6 is expressed in the medial ganglionic eminence (MGE) of the embryonic telencephalon (Fig. 1A,B), where it is coexpressed with both Nkx2-1 and Dlx1/2 (Du et al., 2008; Fogarty et al., 2007; Wang et al., 2010). Shh induces expression of *Nkx2-1* (Flandin et al., 2011), which in turn directly activates *Lhx6* expression (Du et al., 2008; Sandberg et al., 2016). Nkx2-1, in turn, cooperates with Lhx6 to directly activate expression of multiple other genes that control cortical interneuron specification and differentiation, including *Sox6* and *Gsx2* (Batista-Brito et al., 2009; Zhao et al., 2008). Furthermore, *Lhx6* is both necessary and sufficient for the tangential migration of the great majority of interneuron precursors from the MGE to their final destinations in cortex and hippocampus (Fogarty et al., 2007; Liodis et al., 2007; Vogt et al., 2014). Finally, Lhx6 expression persists in mature interneurons that express parvalbumin (Pvalb) and somatostatin (Sst), and is necessary for their expression (Liodis et al., 2007).

The functional role of Lhx6 in hypothalamic development has not been previously investigated. However, previous studies imply this may differ in certain key ways from its function in the developing telencephalon. Notably, the hypothalamic domain of Lhx6 expression only partially overlaps with that of *Nkx2-1* (Shimogori et al., 2010). Furthermore, in sharp contrast to cortical interneurons, no overlap of Lhx6 and either Pvalb or Sst expression has been reported in the ZI (Liu et al., 2017). In this study, we sought to determine the extent to which gene regulatory networks controlling development of hypothalamic Lhx6 neurons diverge from those that control development of telencephalic Lhx6 neurons. We find that hypothalamic Lhx6 regulates neuronal differentiation and survival. Combinatorial

patterns of transcription factor expression delineate spatial subdomains of Lhx6 expression within the ID/TT, and we find that *Nkx2-1*, *Nkx2-2*, and *Dlx1/2* each regulate expression of Lhx6 in largely non-overlapping domains. Finally, we observe extensive molecular heterogeneity among mature hypothalamic Lhx6 neurons, and a lack of overlap with annotated subtypes of Lhx6-expressing cortical interneurons, These findings highlight key similarities and differences between the regulation and function of Lhx6 in hypothalamus and telencephalon.

Results:

Our previous work has indicated that Lhx6 is expressed in two continuous yet distinct domains of the developing hypothalamus: the intrahypothalamic diagonal (ID) and the more posterior tuberomamillary terminal (TT) (Bedont et al., 2015; Shimogori et al., 2010). We next sought to more carefully determine the expression pattern of Lhx6 and its putative regulators during early hypothalamic development. High-quality chromogenic *in situ* hybridization (ISH) detects both the ID and TT domain of Lhx6 expression at E11.5, E12.5 and E14.5 (Fig. 1A-F). By E16.5, hypothalamic Lhx6-expressing cells are observed in the zona incerta (ZI) and dorsomedial hypothalamus (DMH), in a pattern that broadly corresponds to the earlier ID domain, while expression in the posterior hypothalamus (PH) and lateral hypothalamus (LH) in turn broadly corresponds to the TT domain (Fig. 1G, H). This closely matches the pattern of hypothalamic Lhx6 expression previously reported in adults (Liu et al., 2017). Parasagittal sections of adult Lhx6-eGFP BAC transgene expression, which faithfully recapitulates endogenous *Lhx6* expression (Liu et al., 2017), reveal a moderately compact domain of Lhx6 expression in PH, where small numbers of more broadly distributed Lhx6-expressing cells (Fig. 1K, L). Lhx6-expressing neurons are only a small minority of hypothalamic GABAergic neurons (Liu et al., 2017), with scRNA-Seq revealing that only ~2% of all hypothalamic GABAergic neuronal precursors (defined by *Gad1/2* and *Dlx1/2* expression) express *Lhx6* between E11 and E13 (Fig. 1M) (D. W. Kim et al., 2019).

This regional pattern of hypothalamic *Lhx6* expression is broadly similar to that reported for *Lhx6*$^{Cre/+;}$*Ai9* mice (Liu et al., 2017) (Fig. S1), with ~65-70% of tdTomato-expressing neurons in ZI, DMH and PH of *Lhx6*$^{Cre/+;}$*Ai9* adult mice also continuing to express Lhx6. Notably, we see few tdTomato-expressing neurons in other hypothalamic regions, with largest numbers found in adjacent structures such as the VMH (surrounding VMH) and LH, although only ~5% of these tdTomato-expressing neurons also still express Lhx6 (Fig. S1). This shows that, in contrast to telencephalic interneuron precursors, hypothalamic Lhx6 cells do not appear to undergo long-distance tangential migration, and that hypothalamic Lhx6-expressing cells that do undergo short-range tangential dispersal during early development generally repress Lhx6 expression as they mature. These findings led us to investigate other potential differences in Lhx6 function in hypothalamic neurons relative to telencephalon. While Lhx6 does not regulate the survival of cortical interneuron precursors (Liodis et al., 2007), hypothalamic-specific loss of function of

Lhx6 leads to substantial changes in sleep patterns, raising the possibility that Lhx6 may be necessary for the viability of these neurons.

To investigate this possibility, we tested P8 *Lhx6*$^{CreER/CreER}$ mice, in which a CreER cassette has been inserted in frame with the start codon to generate a null mutant of *Lhx6*, to determine if read-through transcription of endogenous *Lhx6* could be detected in hypothalamus (Fig. 2A). Chromogenic *in situ* hybridization of telencephalic structures such as amygdala and cortex reveals that Lhx6-expressing cells are still detected in both regions, although the number of Lhx6-expressing cells in the cortex is substantially reduced in *Lhx6*$^{CreER/CreER}$ mice relative to *Lhx6*$^{CreER/+}$ heterozygous controls (Fig. 2B-M). This is consistent with the severe reduction in tangential migration of cortical interneurons seen in *Lhx6*-deficient mice (Liodis et al., 2007; Vogt et al., 2014). In the hypothalamus, however, no read-through transcription of *Lhx6* was detected (Fig. 2J, M). This implies that, in contrast to its role in the telencephalon where *Lhx6* is necessary for the tangential migration and proper laminar positioning (Vogt et al., 2014; Zhao et al., 2008) , hypothalamic *Lhx6* is required to promote neuronal survival and/or to activate its own expression.

To distinguish between these possibilities, we sought to determine whether neonatal loss of function of *Lhx6* would lead to the death of Lhx6-expressing cells. This was done using genetic fate mapping of *Lhx6*-deficient neurons. Using a series of 4-hydroxytamoxifen injections between P1 and P5 in *Lhx6*$^{CreER/+}$*Ai9* and *Lhx6*$^{CreER/lox}$*;Ai9* mice, we labeled *Lhx6*-expressing cells with tdTomato while also simultaneously disrupting *Lhx6* function in a subset of Lhx6-expressing neurons in *Lhx6*$^{CreER/lox}$ mice (Fig. 3a). We then quantified the number of cells that expressed both tdTomato and Lhx6 protein at P45, as well as the number of cells that only expressed tdTomato. Expression of only tdTomato indicates that a cell has lost expression of Lhx6, either as a result of Cre-dependent disruption of the Lhx6 locus or as a result of normal repression of expression during postnatal development. In both hypothalamic and telencephalic regions in *Lhx6*$^{CreER/+}$*;Ai9* mice, we observed that the fraction of cells that only express tdTomato was only 10-15% of the number of cells expressing both Lhx6 and tdTomato (Fig. 3b). This indicates that the great majority of cells in both regions that express *Lhx6* in neonates continue to do so at P45. However, when we performed this same analysis in *Lhx6*$^{CreER/lox}$*;Ai9* mice, we found that while 75% of tdTomato-expressing cells in the cortex and amygdala remain even in the absence of detectable Lhx6 protein, a substantially smaller fraction of tdTomato-expressing neurons are detected in the absence of Lhx6 protein in the ZI, DMH, and PH.

This is consistent with *Lhx6* playing a selective role in regulating the survival of Lhx6-expressing hypothalamic neurons. To directly address this hypothesis, we next generated *Lhx6*$^{CreER/lox}$*;Bax*$^{lox/lox}$*;Ai9* mice, with loss of function of *Bax* predicted to selectively prevent apoptosis in Lhx6-expressing cells (Takeuchi et al., 2005). When Cre recombinase activity was induced using the same protocol, we observed that the fraction of tdTomato-expressing cells that lacked Lhx6 expression was indistinguishable from that seen in cortex and amygdala (Fig. 3C, Fig. S2).

These data indicate that Lhx6 is selectively required for survival of hypothalamic Lhx6^{+} neurons. To determine whether *Lhx6* is also required for normal differentiation of these cells, we next conducted RNA-Seq analysis on sorted tdTomato-expressing hypothalamic cells from - P10 *Lhx6*$^{CreER/+}$*;Ai9* and *Lhx6*$^{CreER/lox}$*;Bax*$^{lox/lox}$*;Ai9* mice (Fig. 4A). We observe that *Lhx6*$^{CreER/lox}$*;Bax*$^{lox/lox}$*;Ai9* mice show no change in expression of markers of GABAergic neurons, including *Gad1*, *Gad2*, *Slc32a1*. However, substantially increased expression of genes expressed in mitotic neural progenitors, including *Ccna1*, *Aurka, Msx1,* and *Msx2* (Fig. 4b), is observed, along with decreased expression of axon guidance/growth factors such as *Sema3c*, *Sema4d*, *Sema5a*. Notably, we also observe ectopic expression of genes that are not normally found in the brain, but expressed in germline stem cells (*Sycp1*), testes (*Ccdc144b, Samd15, Stag3*) mucosa (*Slc12a8*), colon (*Nlrp6*), liver (*Tfr2*), heart (*Popdc2, Spta1*), cochlear hair cells (*Pdzd7*) (Ling et al., 2020). This suggests that, as in telencephalic neurons, Lhx6 is not required for expression of GABAergic markers (Liodis et al., 2007; Vogt et al., 2014)(Vogt et al., 2014; Zhao et al., 2008)(Liodis et al., 2007; Vogt et al., 2014), but may be required to repress inappropriate expression of genes expressed both in neural progenitor and in non-neuronal cells, although does not exclude the possibility that these may be in part induced as result of loss of function of *Bax*.

Genetic and biochemical analysis have identified a number of genes as direct or indirect Lhx6 targets in the developing telencephalon (Denaxa et al., 2012; Flandin et al., 2011; Sandberg et al., 2016; Vogt et al., 2014; Zhao et al., 2008). These include *Shh*, the transcription factors *Arx*, *Cux2*, *Mafb*, *Nkx2-1*; as well as *Sst* and chemokine receptors such as *Cxcr4*, *Cxcr7*, and *Erbb4*. To identify genes and signaling pathways that are strong candidates for selectively regulating survival of hypothalamic Lhx6 neurons, the bulk RNA-Seq data from P10 *Lhx6*$^{CreER/+}$*;Ai9* neurons was directly compared to profiles obtained from FACS-isolated *Lhx6-GFP* positive and negative hypothalamic and cortical neurons that were collected at P8 (Fig. 4C). Genes found to be enriched in hypothalamic samples of bulk RNA-Seq data were then compared to single-cell RNA-Sequencing (scRNA-Seq) datasets of hypothalamic Lhx6-expressing neurons collected at E15.5 and P8 (D. W. Kim et al., 2019)(Fig. 4C), and a core set of Lhx6-regulated genes that were selectively enriched in hypothalamic Lhx6-expressing neurons was thus identified.

We observe that many previously identified Lhx6 targets either show little detectable expression in wildtype hypothalamic Lhx6 cells, (*Cux2*, *Mafb*, *Sst*, *Cxcr4/7*) or else showed no detectable change in expression following *Lhx6* loss of function (*Arx*, *Nkx2-1*). One notable exception is the Neuregulin receptor *Erbb4*, which has been shown to be necessary for tangential migration and differentiation of MGE-derived immature Lhx6-expressing cortical interneurons (Bartolini et al., 2017; Flames et al., 2004; Li et al., 2012). *Erbb4* is both highly expressed in hypothalamic Lhx6 neurons, and is strongly *Lhx6*-dependent (Fig. 4B). Since Neuregulin signaling is also neurotrophic in many cell types (Mei and Xiong, 2008), this suggested that the loss of neuregulin signaling could be a potential mechanism behind the apoptotic death of *Lhx6*-deficient hypothalamic cells. Indeed, we observed that additional components of the both the Neuregulin (*Nrg1*) and Gdnf (*Ret, Gfra1, Gfra2*)

neurotrophic signaling pathways were selectively enriched in hypothalamic Lhx6 neurons (Fig. 4D, E), a finding which was confirmed using fluorescent *in situ* hybridization and scRNA-Seq (Fig. S3).

We next sought to comprehensively investigate similarities and differences in gene expression and chromatin accessibility in age-matched hypothalamic and telencephalic Lhx6-expressing cells (Fig. 5), and to identify transcription factors that might control their development. Using *Lhx6-GFP* mice, which faithfully recapitulate the endogenous expression pattern of *Lhx6* (Liu et al., 2017), we integrated bulk RNA-Seq analysis obtained at E15 and P0 from hypothalamus and cortex with age-matched ATAC-Seq data (Fig. 5a). At E15, many region-specific differences in gene expression were observed, particularly for transcription factors. We observed enriched expression of *Six3*, *Nkx2-2*, *Nkx2-4* in hypothalamus. As predicted by earlier studies, we observed enriched expression of the telencephalic marker *Foxg1*, as well as *Satb2* and *Nr2e1 (Stenman et al., 2003; Wonders et al., 2008)*, in cortex (Fig. 5B, Table S2).

However, expression of genes broadly expressed in GABAergic neurons showed no significant differences, including *Nkx2-1* and *Dlx1/2*. At P0, hypothalamic Lhx6 cells continued to show enriched expression for multiple transcription factors, including *Prox1*, *Foxp2*, and *Nhlh2*. Hypothalamic Lhx6 cells show little detectable expression of the cortical interneuron markers *Pvalb, Sst* and *Npy*, but we observed a higher level of galanin (*Gal*) and prepronociceptin (*Pnoc*) at P0 in hypothalamic Lhx6 cells. Relative to *Lhx6*-negative hypothalamic cells, we also observed a higher level of transcription factors such as *Dlx1*, *Onecut1*, *Pax5*, and *Nkx2-2* in hypothalamic Lhx6 cells compare to the rest of the hypothalamus at E15.5, as well as higher level of *Tac1* and *Pnoc* at P0 (Fig. S4, Table S3).

Regions of accessible chromatin identified by ATAC-Seq were, as expected, clustered in the proximal promoter and intronic regions of annotated genes in all samples profiled (Fig. S5). Region-specific differences in chromatin accessibility frequently corresponded to differences in mRNA expression. For instance, proximal promoter and/or intronic regions of *Foxg1, Npy, Pvalb,* and *Sst* were selectively accessible in cortical Lhx6 neurons, while those of *Nkx2-2, Sall3,* and *Gal* were accessible only in hypothalamus at both E15 and P0 (Fig. 5B, Table 4, 5, Fig. S5). However, substantial differences in chromatin accessibility was also observed for *Nkx2-1* and *Dlx1/2* at both E15 and P0, implying that different gene regulatory networks may control expression of these genes in hypothalamus and cortex (Table 4, 5).

Since hypothalamic Lhx6 cells express different sets of transcription factors than telencephalic Lhx6-expressing cells, and show differing patterns of chromatin accessibility in hypothalamus and cortex, we reasoned that specific transcription factors might selectively control Lhx6 expression in restricted spatial domains of the developing hypothalamus. Based on both bulk and scRNA-Seq data, as well as previous work, we selected three transcription factors for functional analysis: *Nkx2-1*, *Dlx1/2,* and *Nkx2-2*. *Nkx2-1* is required for Lhx6 expression in the telencephalon (Du et al., 2008; Sandberg et al., 2016) and is expressed in the TT but not ID domain in

the hypothalamus (D. W. Kim et al., 2019; Shimogori et al., 2010), while *Dlx1/2* are required for tangential migration of cortical interneurons and are also broadly expressed in both cortical and hypothalamic Lhx6 cells (Anderson et al., 1997; Bulfone et al., 1993; Colasante et al., 2008; Shimogori et al., 2010). *Nkx2-2*, in contrast, is expressed only in the hypothalamus in a zone immediately dorsal to the region of Nkx2-1 expression (Fig5H-L) (Shimamura et al., 1995; Shimogori et al., 2010).

Each of these transcription factors are expressed in discrete spatial domains that overlap with distinct subsets of hypothalamic Lhx6 cells at E13.5 (Fig. 5C-Q). *Dlx1* was strongly expressed in the ID (Fig. 5C-G, Fig. S6A-D, Fig. S7A-C), but not the TT. Nkx2-2, in contrast, selectively demarcated the region joining the ID and TT (Fig. 5H-L), which we have termed the hinge domain. Nkx2-1 was selectively expressed in the TT region, but essentially absent from the ID and hinge domain (Fig. 5M-Q). These spatial differences in the expression of Dlx1 and Nkx2-1 in hypothalamic Lhx6 cells are preserved at E17.5, where *Dlx1* is enriched in the more anterior ZI and DMH (Fig. S6), and *Nkx2-1* expression is enriched in the PH (Fig. S6G'-J'). Dlx1 and Nkx2-1 formed mutually exclusive expression domains in the ID and TT (Fig. S7D-F). However, we observed a much more even distribution of Nkx2-2/Lhx6 cells across the ZI, DMH and PH, which could indicate either short-range tangential dispersal of hinge cells, or widespread induction of Nkx2-2 expression in Lhx6 cells at later ages (Fig. S6M-X). These results indicate that distinct spatial domains of hypothalamic Lhx6 expression can be delineated by combinatorial patterns of homeodomain transcription factor expression.

To determine the final location of *Nkx2-1* expressing Lhx6 cells, we next used fate-mapping analysis, in which *Nkx2-1*$^{CreER/+}$*;Ai9* mice (Taniguchi et al., 2011) were labeled with 4-OHT at E11 (Fig. S8A). At E18, tdTomato^{+} expression was detected in the majority of Lhx6-expressing cells in the amygdala and cortex (Fig. S8) as expected (Du et al., 2008; Sandberg et al., 2016), but we observed anterior-posterior bias in distribution of tdTomato^{+} cells in the hypothalamus that closely matched the location of Lhx6/Nkx2-1 expressing cells at earlier ages. We observe that only a small fraction (~10%) of ZI Lhx6-expressing cells, which correspond to the most anterior region of Lhx6 expression at later developmental ages (Liu et al., 2017), were labelled with tdTomato. In contrast, a much larger fraction of PH Lhx6 cells, corresponding to the most posterior domain of Lhx6 expression, were expressing tdTomato. This implies that Nkx2-1/Lhx6-expressing cells of the TT primarily give rise to Lhx6 cells found in the posterior hypothalamus, but that a small fraction may undergo tangential migration to more anterior structures such as the ZI.

To further identify these anatomically and molecularly distinct Lhx6-expressing domains in the developing hypothalamus, we performed single-cell RNA sequencing (scRNA-Seq) with the *Lhx6-GFP* line at E12.5, and E15.5. At E12.5 and E15.5, scRNA-Seq analysis readily distinguishes the ID, TT and hinge domains (Fig. 6, Fig. S9-S11). In addition, weak *Lhx6* expression was observed in Lhx1 and Lhx8-expressing cells of the anterior ID cluster, which are *Nkx2-1*+ (Fig. 6B), and give rise to GABAergic neurons in the suprachiasmatic nucleus and DMH, although little or no *Lhx6* mRNA was detected in these cells after E13.5 (Bedont et al., 2014;

Shimogori et al., 2010)(Fig. 6, Fig. S9-S11). We observed that *Dlx1/2*, *Nkx2-2* and *Nkx2-1* are differentially expressed in the ID, hinge, and TT domains, respectively, at both ages (Fig6, Fig. S9-S11), as previously shown by immunostaining and *in situ* hybridization. We observe several molecularly distinct cell clusters that have not been previously described. The first cluster expresses low levels of *Nkx2-1*, but high levels of *Prox1* and *Sp9*, transcription factors that are highly expressed in the developing prethalamus, and may correspond to a dorsal subdomain of the TT located adjacent to the hinge domain (Fig. 6A-C). We also observe a distinction between more proximal and distal domains of the ID, based on expression of *Nefl, Dlx6, Nefm, Lhx1* and *Nr2f1*.

In all, five molecularly distinct clusters of neurons that strongly express Lhx6 could be resolved in the embryonic hypothalamus (Fig. 6). These can be distinguished not only by expression of different subsets of transcription factors at E12.5, but also by more conventional markers of cell identity such as neuropeptides and calcium binding proteins such as *Sst, Tac1, Pnoc, Islr2, Gal, Npy* at E15.5 (Fig. S11, Table. S6-8). We also observed clusters that were expressed in the hinge and TT region at E12.5 (Fig. S11 cluster 4 and 7), but also expressed markers that are restricted to neurons at the most anterior domain of hypothalamic Lhx6 neurons in the early neonatal period. These include *Nfix*, *Nfib* and *Tcf4* (Fig. S11, Fig. 8, Table. S6-8).

These molecularly distinct domains of hypothalamic Lhx6 neurons were also visualized using traditional two-colour ISH (Fig. S12), with *Nkx2-1, Nkx2-2, Arx,* and *Prox1* (Fig. S12). This also confirms that *Shh* is only expressed in dorsal TT Lhx6 neurons, while *Six3* is expressed only in the weakly Lhx6-expressing cells in the anterior ID. ScRNA-Seq showed that *Lef1,* which is expressed broadly in the ID and TT region at E12.5, was expressed in only very few Lhx6 cells at both E12.5 and E15.5 (Fig. 6, Fig. S12), indicating that *Lef1* and *Lhx6* are not extensively co-expressed. This is not evident using two-color ISH.

To determine whether any of these spatial domains of Lhx6 expression more closely resembled telencephalic Lhx6 cells, we compared these E12.5 hypothalamic scRNA-Seq results to data previously obtained from E13.5 MGE (Mayer et al., 2018). These data confirmed that, while transcription factors such as *Nkx2-1*, *Dlx1/2*, and *Lhx8* are broadly expressed in Lhx6 MGE cells, they are not expressed (*Lhx8*) or expressed only in discrete subsets (*Nkx2-1*, *Dlx1/2*) of hypothalamic Lhx6 neurons. No identified subset of hypothalamic Lhx6 neurons obviously resembled MGE Lhx6 cells (Fig. 6, Table. S6-8).

We next investigated whether loss of function of *Nkx2-1*, *Nkx2-2* and *Dlx1/2* led to loss of spatially-restricted hypothalamic expression of Lhx6. We first examined *Nkx2-1*$^{CreER/CreER}$ mice, in which targeted insertion of the CreER cassette generates a null mutation in *Nkx2-1* (Taniguchi et al., 2011). This leads to severe hypoplasia of the posteroventral hypothalamus, as previously reported for targeted *Nkx2-1* null mutants (Marín et al., 2002). The ventrally-extending TT domain of Lhx6 expression is not detected in *Nkx2-1*-deficient mice at E12.5, but the Nkx2-1-negative ID domain persists (Fig. 7, Fig. S13). Fate mapping analysis, in which

Nkx2-1$^{CreER/+}$*;Ai9* and *Nkx2-1*$^{CreER/CreER}$*;Ai9* mice were injected with tamoxifen at E11 and analyzed at E18, indicate that surviving Lhx6 cells in the ID region represent a mixture of tdTomato positive and negative cells, and confirm that a subset of these surviving cells derived from *Nkx2-1*-expressing precursors. As previously reported, no Lhx6-expressing cells are detected in the mutant cortex (Fig. S14).

We next generated null mutants of *Nkx2-2* in the same manner, generating mice homozygous for a knock-in CreEGFP cassette that disrupts expression of the endogenous *Nkx2-2* locus (Balderes et al., 2013). In this case, we observe a loss of Lhx6 expression in the hinge region, located between the posterior ID and dorsal TT (Fig. 7, Fig. S13). Finally, we examined the phenotype of mice deficient for *Dlx1/2*, examining both global knockouts (Qiu et al., 1997) and *Foxd1*$^{Cre/+}$*;Dlx1/2*$^{lox/lox}$ mutants (Silbereis et al., 2014), in which *Dlx1/2* are selectively deleted in hypothalamic and prethalamic neuroepithelium (Liu et al., 2017; Newman et al., 2018; Salvatierra et al., 2014). In both global and diencephalic-specific *Dlx1/2* knockouts, the ID domain of Lhx6 expression is absent at E12.5, whereas the TT domain is intact. At E17, we also observe a major reduction in the number of Lhx6-expressing cells in the ZI (Fig. S15). These results indicate that spatially discrete domains of hypothalamic Lhx6 expression are controlled by expression of different transcription factors (Fig. S13).

Since Lhx6 cells in the embryonic hypothalamus are both transcriptionally diverse and divergent from telencephalic Lhx6 cells, we hypothesized that identified subtypes of Lhx6 neurons in the postnatal hypothalamus would likewise diverge substantially from those present in the cortex (Tasic et al., 2016). ScRNA-Seq analysis of P8 Lhx6-eGFP cells from hypothalamus that expressed high levels of Lhx6 mRNA shows that these cells express a diverse pool of neuropeptides and neurotransmitters that are not expressed in telencephalic Lhx6 neurons, including *Gal*, and *Trh* (Fig. 8, Fig. S16, S17). Other markers that are specific to distinct subsets of cortical Lhx6 cells were expressed in hypothalamic Lhx6 neurons, such as *Pnoc*, *Tac1, Nos1*, and *Th*. Hypothalamic Lhx6 cells do not express *Pvalb*, but a small fraction express *Npy* and *Cck*. We also identified a rare subpopulation of hypothalamic Lhx6 cells in the PH that co-express *Sst*, although these are absent in more anterior regions (Fig. S16). *Tac1* is expressed broadly in cortical and hypothalamic Lhx6 cells. Similar patterns of gene expression are observed in scRNA-Seq data obtained from Lhx6 neurons in the adult hypothalamus (Fig. 18) (D. W. Kim et al., 2019; Mickelsen et al., 2019; Rossi et al., 2019). However, all these enriched markers (neuropeptides and neurotransmitters) are not specific to Lhx6 neurons but rather expressed broadly in hypothalamic GABAergic neurons (Fig. S19).

Mature Lhx6 hypothalamic neurons were organized into three major clusters that showed close similarity to the two subdomains of the ID and the main TT region observed at E12.5, and in turn appear to represent individual subtypes of Lhx6 neurons that are differentially distributed along the anteroposterior axis of the hypothalamus, and which may correspond to Lhx6 neurons of the ZI, DMH and PH, respectively (Fig. S20). Lhx6 neurons express a mixture of *Pnoc*, *Penk*, *Calb1*, *Calb2*, *Cck* across ZI and DMH, whereas *Tac1* is more restricted to the ZI. *Npy* and

Nos1 are enriched in DMH Lhx6 neurons. *Th*, *Trh*, *Gal* are located in the region spanning the DMH and PH, while *Sst* is expressed only in a small subset of PH Lhx6 neurons.

Discussion:

The LIM homeodomain factor Lhx6 is a master regulator of the differentiation and migration of GABAergic neurons of the cortex and hippocampus, as well as many other subcortical telencephalic structures such as striatum and amygdala (ref, ref). Over 70% of cortical interneurons express Lhx6 into adulthood, where it is required for expression of canonical markers of interneuron subtype identity such as Sst and Pvalb (Denaxa et al., 2012; Tasic et al., 2016). In contrast, Lhx6 is expressed in only 1-2% of hypothalamic GABAergic neurons. Lhz6 expression is confined to a broad domain in the dorsolateral hypothalamus, and Lhx6-expressing cells do not undergo widespread long-distance tangential migration. Lhx6-expressing hypothalamic neurons in the ZI play an essential role in promoting sleep (Liu et al., 2017), but their function is otherwise uncharacterized. In this study, we seek to characterize similarities and differences between the development and molecular identity of telencephalic and hypothalamic Lhx6 neurons.

In hypothalamus, in sharp contrast to telencephalon, Lhx6 is required to prevent neuronal apoptosis. The fact that loss of function of hypothalamic Lhx6 leads to death of sleep-promoting cells in the zona incerta may account for the more severe changes in sleep pattern that is seen in hypothalamic-specific loss of function of Lhx6 than is observed following DREADD-based manipulation of the activity of these neurons (Liu et al., 2017). Analysis of *Lhx6*/*Bax* double mutants identified both the Neuregulin and Gdnf signaling pathways as potential neurotrophic mechanisms that promote survival of hypothalamic Lhx6 neurons. Interestingly, Nrg1/ErbB4-dependent signaling acts a chemorepellent signal, while Gdnf signaling acts a chemoattractant, and both regulate the tangential migration of cortical Lhx6 neurons (Li et al., 2012; Pozas and Ibáñez, 2005). Thus, both signaling pathways appear to have been repurposed in the context of hypothalamic development.

We observe extensive transcriptional divergence between developing telencephalic and hypothalamic Lhx6 neurons. Notably, we observe clear spatial differences in gene expression among hypothalamic Lhx6 neurons that are not detectable in the MGE. While MGE cells require *Nkx2-1* to activate *Lhx6* expression, *Nkx2-1* is expressed primarily in the TT, in the posterior region of hypothalamic Lhx6 expression. TT domain also expresses *Shh* similar to MGE and may regulate *Nkx2-1* expression (Abecassis et al., n.d.; Flandin et al., 2011), which could activate Lhx6 expression. We fail to observe any upstream gene expression (*Shh* or *Nkx2-1*) in MGE scRNA-Seq clusters when the downstream gene is detected (*Nkx2-1* or *Lhx6*)(Mayer et al., 2018), indicating *Nkx2-1* and *Lhx6* activation could lead to shutdown of *Shh* and *Nkx2-1* in the MGE. However in our scRNA-Seq, all three genes (*Shh*, *Nkx2-1* and *Lhx6*) are highly co-expressed in TT domain. Maintenance of *Nkx2-1* expression partly resembles Lhx6 projection neurons in the subpallium including lack of tangential migration, but hypothalamic Lhx6 neurons in the ID and

TT both lack *Lhx8* expression (Flandin et al., 2011)(Abecassis et al., n.d.; Flandin et al., 2011)(Flandin et al., 2011). Likewise, *Dlx1/2* are expressed in virtually all Lhx6-expressing MGE cells, but are not required to maintain *Lhx6* expression (Sandberg et al., 2016; Zhao et al., 2008), while *Dlx1/2* are primarily expressed in the ID domain in hypothalamus. Furthermore, *Nkx2-2* is not expressed in the telencephalon, but is selectively expressed in a previously uncharacterized hinge domain that connects the ID and TT. We find that mutants in *Nkx2-1*, *Nkx2-2* and *Dlx1/2* selectively eliminate hypothalamic Lhx6 expression in the TT, hinge and ID domains, respectively. This indicates a high level of spatial patterning and transcriptional diversity among developing hypothalamic Lhx6 neurons. Although hypothalamic Lhx6 cells do not undergo extensive tangential dispersal, like in telencephalon, lineage analysis indicates that by E18, a subset of cells that express the TT-specific marker Nkx2-1 have migrated to anterior structures such as the ZI. Combined with the observation that Nkx2-2 expression progressively spreads outward from the hinge domain, this implies that subsets of hypothalamic Lhx6 cells may undergo short-range migration during development.

Lhx6 neurons in the postnatal hypothalamus are likewise highly transcriptionally diverse, and do not directly correspond to any of their telencephalic counterparts. No hypothalamic Lhx6 cells express *Pvalb*, and only a few selected subsets express either *Sst* or *Npy*. In the cortex, there are many genes that are exclusively expressed in Lhx6-expressing neurons -- including *Sst*, *Pvalb*, and *Npy*. In contrast, in the hypothalamus, no genes were identified that were exclusively expressed in Lhx6 neurons, other than *Lhx6* itself. Neuropeptides such as *Pnoc*, which are expressed in large subsets of hypothalamic Lhx6 neurons, are also widely expressed in many cells that do not express Lhx6. Finally, molecularly distinct subtypes of Lhx6 neurons are broadly and evenly distributed in the cortex, owing to the widespread tangential dispersal during development. In contrast, in the hypothalamus, we observe clear differences in the expression of neuropeptides and calcium binding proteins in Lhx6 neurons that broadly correspond to the spatial position of these cells.

These results provide a starting point to not only better define the molecular mechanisms that control differentiation, survival and diversification of hypothalamic Lhx6 neurons, but also serve as a molecular toolbox for selectively targeting molecularly distinct neuronal subtypes. Previous studies identified Lhx6 neurons of the zona incerta as being unique in promoting both NREM and REM sleep (Liu et al., 2017). Identification of molecular markers that distinguish different subtypes of Lhx6 cells in this region can help determine whether this is actually produced by activation of distinct neuronal subtypes. Hypothalamic Lhx6 neurons also send and receive connections from many brain regions that regulate innate behaviors, including the amygdala, periaqueductal grey, and ventral tegmental area (Liu et al., 2017). The function of these circuits is as yet unknown, and the molecular markers identified in this study can serve as a starting point for investigating their behavioral significance.

Acknowledgements: This work was supported by a grant from the NIH (R01DK108230) to S.B, the Maryland Stem Cell Research Fund to DWK, and the Japan Society for the Promotion of Science to T.S. We thank Transcriptomics and Deep Sequencing Core (Johns Hopkins) for sequencing of bulk RNA-Seq, bulk ATAC-Seq and scRNA-Seq libraries, and Ross Flow Cytometry Core (Johns Hopkins) for flow sorting of *Lhx6-GFP* cells, and Microscope facility (Johns Hopkins MICFAC, supported by the award number S10OD018118). We thank Wendy Yap for comments on the manuscript.

Contribution: SB conceived study. DWK, KL, SB designed experiments. DWK, KL, ZQW, SZ, AB, MPB, SHL, PWW, performed experiments. DWK, KL, ZQW, SZ, PWW analyzed data. All authors contributed to writing the paper.

Data availability: All sequencing data are available on GEO, GSE150687.

Materials and Methods:

Mice

All experimental animal procedures were approved by the Johns Hopkins University Institutional Animal Care and Use Committee. All mice were housed in a climate-controlled facility (14-hour dark and 10-hour light cycle) with *ad libitum* access to food and water.

Lhx6-GFP (Tg(Lhx6-EGFP)BP221Gsat) (Gong et al., 2003), *Lhx6*^{CreER} knock-in (B6(Cg)-*Lhx6tm1*($^{cre/ERT2}$)*Zjh*/J, JAX #010776) (Taniguchi et al., 2011), *Lhx6*$^{lox/lox}$ (Denaxa et al., 2018), *Ai9* (B6.Cg-*Gt(ROSA)26Sortm9(CAG-tdTomato)Hze*/J, JAX #007909) (Madisen et al., 2010), *Bax*$^{lox/lox}$ (B6;129-*Baxtm2Sjk Bak1tm1Thsn*/J, JAX #006329) (Takeuchi et al., 2005), *Nkx2-2*^{CreGFP} (B6.129S6(Cg)-*Nkx2-2tm4.1(cre/EGFP)Suss*/J, JAX #026880) (Balderes et al., 2013), *Nkx2-1*^{CreER} (*Nkx2-1tm1.1(cre/ERT2)Zjh*/J, JAX #014552) (Taniguchi et al., 2011), *Foxd1*^{Cre} (B6;129S4-*Foxd1tm1(GFP/cre)Amc*/J, JAX #012463) (Humphreys et al., 2010), *Dlx1/2*$^{lox/lox}$ (*Dlx1tm1Rth Dlx2tm1.1Rth*/J, JAX #025612) (Silbereis et al., 2014), *Dlx1/2*$^{-/-}$ (gift from John Rubinstein) were used. Mice were time-mated and embryos at various ages (embryonic day (E)11.5, E12.5, E13.5, E15.5, E16.5, E17.5, E18.5, and postnatal day (P) 8) were collected for high-throughput sequencing and histology. Day of birth was considered as P0.

Tamoxifen injection

Lhx6^{CreER} *pulse-chase experiments*

Pups with parental crosses of *Lhx6*$^{CreER/+}$*;Lhx6*$^{lox/+}$*;Bax*$^{lox/+}$*;Ai9* x *Lhx6*$^{CreER/+}$*;Lhx6*$^{lox/+}$*;Bax*$^{lox/+}$*;Ai9* were treated with intraperitoneal 4-Hydroxytamoxifen injection (4-OHT, 0.5 mg/per day, in corn-oil) for 5 consecutive days between P1 and P5. Pups were genotyped on the day of the birth and 3 different genotypes (1. *Lhx6*$^{CreER/+}$*;Ai9*, 2. *Lhx6*$^{CreER/+}$*; Lhx6*$^{lox/+}$*;Ai9*, 3. *Lhx6*$^{CreER/+}$*;Lhx6*$^{lox/+}$*;Bax*$^{lox/lox}$*;Ai9*) were used. *Lhx6*$^{CreER/CreER}$ genotype dies soon after weaning (Taniguchi et al., 2011), *Lhx6*$^{CreER/+}$*;Lhx6*$^{lox/lox}$ genotype is not possible to generate due to similar sites of *CreER* and *lox* insertion.

Treated pups were collected between P40 and P45 and processed as described below. Cell counting was conducted in all 3 genotypes in the zona incerta (ZI), dorsomedial hypothalamus (DMH), posterior hypothalamus (PH), S1 somatosensory cortex (CTX), amygdala (AMY) following the Mouse Brain Atlas (Watson and Paxinos, 2010). Borders were drawn to separate individual regions using DAPI counterstaining and the Mouse Brain Atlas as a guideline, and 6 500 µm x 500 µm region-of-interest was used to count across cortical layers per section. 3 sections (every second section to avoid counting the same cell) were used per region, and 6 brains that were collected from between 2 and 3 individual litters (different parents) were used. tdTomato expression was observed in blood vessels as previously described (Liu et al., 2017).

Three different types of cells were counted. First, cells that only express Lhx6 protein detected by immunostaining (indicating no 4-OHT-induced Cre recombination). Second, cells that expressed only tdTomato but not Lhx6 (indicating Cre-mediated activation of tdTomato, and disruption of *Lhx6*). Third. cells that expressed both tdTomato and Lhx6 (indicating incomplete 4-OHT-induced Cre recombination, with induction of tdTomato expression and failure to recombine the conditional allele of *Lhx6*). Only cells that expressed tdTomato (with or without Lhx6 protein expression) were counted and the total counted number of cells were used as a denominator. Cells that only expressed tdTomato were used as a numerator to calculate cell survival rate, as we expect to observe a decrease in the ratio (tdTomato$^+$ / (tdTomato$^+$ & tdTomato$^+$/Lhx6$^+$) if *Lhx6* is required for cell survival.

Nkx2-1^{CreER} pulse chase experiments

Nkx2-1$^{CreER/+}$;Ai9 female mice were time-mated to the same genotype male mice, and 4-OHT was intraperitoneally injected (2 mg) at E11.5, and embryos were collected at E18.5

Tissue fixation

Embryos and mice younger than weaning age (P21) were fixed in 4% paraformaldehyde (PFA) between 8 and 12 hours at 4'C, incubated in 30% sucrose overnight at 4'c, and snap-frozen in OCT compound for histology analysis. Whole embryos were used for fixation until E14.5, and from E14.5, brains were dissected out for fixation. Mice older than weaning age were anaesthetised by intraperitoneal injection of avertin and perfused with cold 4% PFA. Brains were post-fixed for 2 hours at 4'C with 4% PFA, and processed as described above.

Cryosection

Frozen brains were sectioned at 25 µm with either a coronal or sagittal plane with a cryostat (Leica CM3050S), and transferred to Superfrost™ Plus slides.

In situ hybridization (ISH)

Chromogenic and fluorescent *in situ* hybridization was performed as previously described to stain for *Lhx6* (BC065077), *Gfra1* (AW060572), *Gfra2* (BE994145), *Ret* (AW123296), *Dlx1* (BC079609), *Calb* (AW489595), Calb2 (AI836013), *Gal* (BC044055), *Penk* (AI836252), *Tac1* (BE954293), *Npy* (AI848386), *Sst* (BE984677), *Th* (BF449409), *Gad1* (AW121495), *Nkx2-1* (BC080868), *Nkx2-2* (BG110), *Shh* (BC063087), *Prox1* (BE982394), *Six3* (BE953775), *Lhx8* (BE448496), *Lef1* (BC038305)(Miranda-Angulo et al., 2014; Shimogori et al., 2010). RNAscope with probe targeting *Lhx6* was tested on E13.5 mice following the manufacturer's protocol. Images were taken under Keyence BZ-X800 fluorescence microscope or Zeiss LSM 700 microscope, and processed with ImageJ (Rueden et al., 2017) and pixel density was measured as previously described (Kim et al., 2016).

Immunostaining

Immunostaining was performed with mouse-anti-Lhx6-antibody (1:200, sc-271433, Santa Cruz), rat-anti-RFP (1:500, ABIN334653, antibodies-online), rabbit-anti-Dlx1 (1:500, gift from Jay Lee), guinea-pig-anti-Dlx1 (1:500, gift from Jay Lee), rabbit-anti-Nkx2-1 (1:500, EP1584Y, Abcam), mouse-anti-Nkx2-2 (1:100, 74.5A5, DSHB), mouse-anti-NeuN (1:2000, MAB377) as previously described (Kim et al., 2016), except that M.O.M blocking reagent (MKB-2213) was used following manufacturer's instruction when mouse primary antibodies were used. Alexa Fluor™ 488, 594, 647 secondary antibodies were used in 1:500 dilutions. Sections were mounted with DAPI-Vectamount (Vectorlabs) and imaged under a Keyence BZ-X800 fluorescence microscope or Zeiss LSM 700 microscope. All cell counting was done with ImageJ. Cell counting was conducted in multiple brain areas across developmental ages using standard reference atlases for orientation (Lein et al., 2007; Shimogori et al., 2010), using DAPI counterstaining or NeuN staining as a guideline. For identification of ID and TT, criteria described in our previous study was used (Shimogori et al., 2010). 3 sections (every second section to avoid counting the same cell, < E15.5 = 2 sections) were used per region, and 4-6 brains collected from between 2 and 3 individual litters were used. Cell counting was conducted blinded.

Bulk RNA-Sequencing

Lhx6 pulse-chase sample sequencing

Lhx6$^{CreER/+}$*;Ai9* and *Lhx6*$^{CreER/+}$*;Lhx6*$^{lox/+}$*;Bax*$^{lox/lox}$*;Ai9* P1 pups were treated with 4-OHT as described above, and collected at P10. Between 4 and 6 pups from 2 different litters were pooled per sample without regard to sex, and papain-based enzymatic dissociation was performed on the dissected hypothalamus as previously described (D. W. Kim et al., 2019). Dissociated cells were flow-sorted for tdTomato signal, and between 25,000 and 30,000 cells were collected directly into TRIzol™ LS reagent. RNA was extracted using Direct-zol RNA kits (Zymo Research) and RNA-Sequencing libraries were made using stranded Total RNASeq library prep. 2 libraries were made for *Lhx6*$^{CreER/+}$*;Ai9*, and 3 libraries were made for *Lhx6*$^{CreER/+}$*;Lhx6*$^{lox/+}$*;Bax*$^{lox/lox}$*;Ai9*. Libraries were sequenced with Illumina NextSeq500, paired-end read of 75 bp, 50 million reads per library. Illumina adapters of sequenced libraries were trimmed using Cutadapt (v1.18)/TrimGalore (v0.5.0) (Martin, 2011) with default parameters, library qualities were assessed using FastQC (v0.11.7)/MultiQC (Ewels et al., 2016). Libraries were then aligned to mm10 using STAR (v2.54b) (Dobin et al., 2013) with --twopassMode Basic. RSEM (v1.3.0) was used for quantification (Li and Dewey, 2011), with rsem-calculate-expression (--forward-prob 0.5). Expected counts value from RSEM was used to perform differential expression using edgeR (v3.24.3) (Robinson et al., 2010) using default parameters except calcNormFactors (method = "TMM").

Lhx6$^{CreER/+}$*;Ai9* or *Lhx6*$^{CreER/+}$*;Lhx6*$^{lox/+}$*;Bax*$^{lox/lox}$*;Ai9* enriched genes (fold change > 2 consistent gene value across replicates), were used with EnrichR (Kuleshov et al., 2016). *Lhx6*$^{lox/+}$*;Bax*$^{lox/lox}$*;Ai9* enriched genes were compared to Mouse Cells and Tissues (MESA) dataset available ascot.cs.jhu.edu (Ling et al., 2020), relying on

robustness of expression (NAUC >20) and specificity, as many of the enriched genes detected in this analysis are not strongly expressed in the developing brain.

We reasoned that the genes showing enriched expression in *Lhx6*$^{CreER/+}$*;Ai9* relative to *Lhx6*$^{CreER/+}$*;Lhx6*$^{lox/+}$*;Bax*$^{lox/lox}$*;Ai9* would be regulated by *Lhx6* and/or *Bax*. Furthermore, since tdTomato expression is detected in blood vessels due to weak Lhx6 expression in endothelial cells during development (Liu et al., 2017), we wanted to enrich expression from Lhx6-expressing cells of the hypothalamus. P8 *Lhx6-GFP*, in which GFP expression is absent in endothelial cells, were used to generate bulk RNA-Sequencing (bulk RNA-Seq) from the cortex and hypothalamus (method described below). Hypothalamus-enriched genes from P8 *Lhx6-GFP* bulk RNA-Seq data were used to enrich genes that are highly expressed in the hypothalamus Lhx6 cells. After enrichment, the gene lists were compared to single-cell RNA-Sequencing (scRNA-Seq) data from P8 *Lhx6-GFP* hypothalamus using the method described below, to further cross-check specificity of expression and to remove any possible contamination that may occurred during flow-sorting from bulk RNA-Seq. EnrichR was used to identify gene pathways, and pathways previously implicated in regulation of neuronal survival were selected.

Lhx6-GFP bulk RNA-Seq

To identify differences between cortical and hypothalamic Lhx6 populations, RNA-Sequencing was performed on E15.5, P0 and P8 *Lhx6-GFP* mice, by collecting 8-10 pups from 2 different litters per library. Libraries were sequenced with Illumina HiSeq 2500, and processed as described in the pipeline described above.

ATAC-Sequencing

Cortex and hypothalamus of E15 and P0 *Lhx6-GFP* mice were collected, dissociated with papain-based enzymatic reaction, and GFP cells were flow-sorted. Between 60,000 and 70,000 cells were collected. Flow-sorted cells were prepared for ATAC libraries as previously described (Buenrostro et al., 2014; Wang et al., 2018). Libraries were sequenced with Illumina NextSeq500, paired-end read of 75 bp, 50 million reads per library. Each sample was run in duplicate.

Illumina adapters of sequenced libraries were trimmed using Cutadapt (v1.18)/TrimGalore (v0.5.0) and library qualities were assessed using FastQC (v0.11.7)/MultiQC. Libraries were aligned to mm10 using Bowtie 2 (v2.25) (Langmead and Salzberg, 2012) using --very-sensitive parameter, and Samtools (v1.9) (Li et al., 2009) was used to check the percentage of mitochondria DNA reads. Picard (v2.18) was used to remove PCR duplicates, and MACS2 (v2.1.2) (Zhang et al., 2008) was used to capture narrow peaks (open chromatin regions) with --shift 100, --extsize 200, --nolambda, --nomodel parameters. ENCODE blacklist regions of the genome were removed using Bedtools (v2.27) intersect function (Amemiya et al., 2019; Quinlan and Hall, 2010; Zhang et al., 2008). Bedtools intersect function was used to find matching peaks between replicates, which the distance of peak ends were less than 10 base pairs. ChIPseeker (v1.18.0) (Yu et al., 2015) was then used to identify regions that were within 3 kb of the transcription start site (TSS).

Footprinting was done using pyDNase (v0.24) (Piper et al., 2015) wellington_footprints function to find transcription factor binding sites and motif analysis was done on footprinting sites with HOMER (v4.11) (Heinz et al., 2010) with default parameters. Peaks between groups were compared as previously described (Buenrostro et al., 2014; Wang et al., 2018) to visualize changes in chromatin accessibility between different ages and brain regions using DiffBind (v.2.10.0) (Ross-Innes et al., 2012) and edgeR using default parameters. Differential peaks were compared to bulk RNA-Seq, and open chromatin peaks in promoter regions that correspond to gene expression were identified to obtain a positive correlation between promoter accessibility and gene expression. Peaks and differential gene expression was then cross-matched to scRNA-Seq, to identify potential different regions within Lhx6 hypothalamic cells that are demarcated by expression of specific transcription factors.

Single-cell RNA-Sequencing

Time-mated E12.5, E15.5 and P8 *Lhx6-GFP* mice were collected, and dissection and dissociated were performed as described previously (D. W. Kim et al., 2019). Between 6 and 10 embryos/pups from 2 different litters were collected. Following dissociation, GFP^+ cells were flow-sorted using Aria IIu Sorter (BD). Between 20,000 and 25,000 cells were flow-sorted for E12 and E15, 2,000 cells were flow-sorted for P8. Flow-sorted cells were used for the 10x Genomics Chromium Single Cell System (10x Genomics, CA, USA) using V3.0 chemistry per manufacturer's instruction. Three libraries were sequenced on Illumina NextSeq 500 with ~200 million reads per library. Sequenced files were processed through the CellRanger pipeline (v3.1.0, 10x Genomics) using mm10 genome.

Seurat V3 (Stuart et al., 2019) was used to perform downstream analysis following the standard pipeline described previously (Bell et al., 2020), analyzing cells that express high *Lhx6* transcript. Louvain algorithm was used to generate different clusters, and spatial information from individual clusters at E12.5 and E15.5 was identified by referring to our previous hypothalamus scRNA-Seq database HyDD (D. W. Kim et al., 2019), as well as previous analysis of anatomical locations of transcription factors (Shimogori et al., 2010). For P8 scRNA-Seq, region-specific transcription factors that are expressed were compared to E12.5 and E15.5 scRNA-Seq gene lists, as well as matching the identified gene lists to the Allen Brain Atlas ISH data (Lein et al., 2007). Previously published scRNA-Seq from E13.5 medial ganglionic eminence (MGE) (Mayer et al., 2018) was processed as described above, and the key markers that label individual clusters were compared to E12.5 Lhx6-expressing hypothalamic cells.

Lhx6$^+$ cells across multiple mutant groups (*Foxd1*$^{Cre/+}$*;Dlx1/2*$^{lox/lox}$*, Nkx2-1*$^{CreER/CreER}$*, Nkx2-2*$^{CreGFP/CreGFP}$) from (D. W. Kim et al., 2019), were used to compare expression level of key transcription factors that define sub-regions of hypothalamic *Lhx6* domains.

Previously generated scRNA-Seq datasets from preoptic region (Moffitt et al., 2018), suprachasmatic nucleus (Moffitt et al., 2018; Wen et al., 2020), ventromedial hypothalamus (D.-W. Kim et al., 2019), and whole hypothalamus (Campbell et al., 2017; Chen et al., 2017; D. W. Kim et al., 2019; Romanov et al., 2017), were analysed as described above. GABAergic neurons (*Slc32a1*$^{+}$) were first subsetted from the dataset, and the percentage of cells expressing *Pnoc*, *Penk*, *Calb1*, *Cck*, *Calb2*, *Gal*, *Tac1*, *Th*, *Npy*, *Trh*, *Sst* was determined.

Statistics

Two-way ANOVA was used for Lhx6 pulse-chase experiments (genotype, brain region). Unpaired t-test was used for other cell counting. The Seurat 'FindAllMarkers' function with 'LR = logistic regression model' with default parameters was used for analyzing differential gene expression, using the number of total mRNAs and genes as a variabile.. All bar graphs show mean and standard error of the mean (SEM), with individual data points plotted.

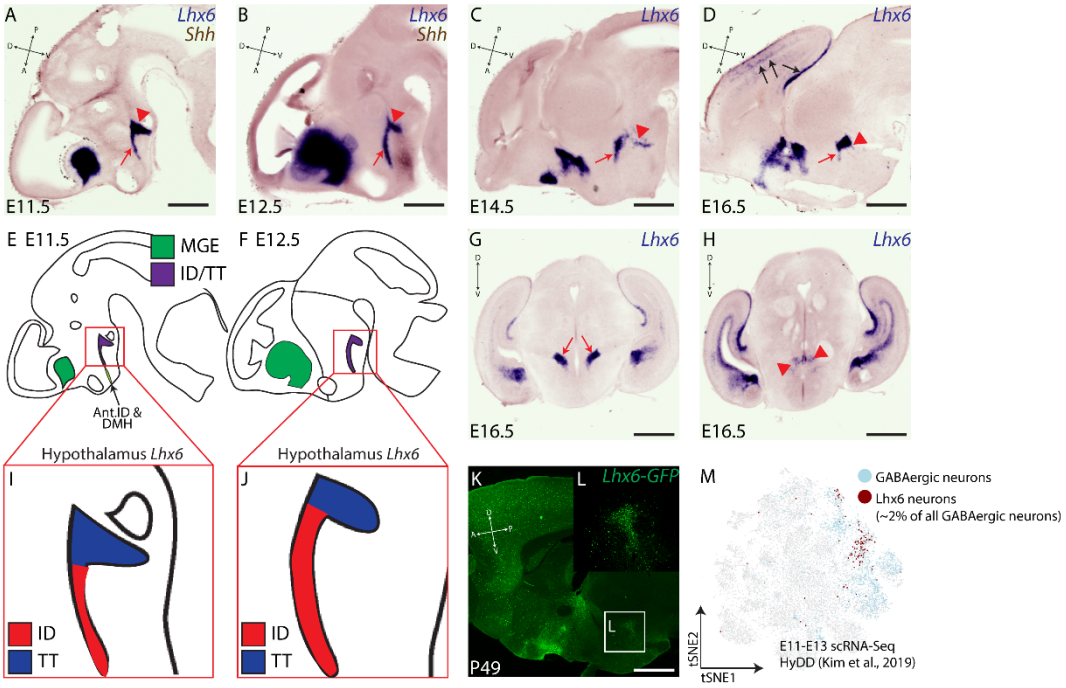

Fig1. Kim, et al.

Figure 1. Lack of migration in hypothalamus *Lhx6*$^+$ cells. (A-D, G, H) *In situ* hybridization showing *Lhx6* (blue) and *Shh* (brown) at E11.5 (A), E12.5 (B), E14.5 (C), E16.5 (D, G, H), shown in sagittal (A-D) and coronal (G,H) planes. Red arrows (A-D) indicate the intrahypothalamic diagonal (ID), red arrowheads (A-D) indicate the tuberomamillary terminal (TT), black arrows (A-D) indicate migrated telencephalic *Lhx6*$^+$ cells (tangential migration from the medial ganglionic eminence to the cortex). (E, F, I, J) Schematics showing distribution of telencephalic (green) and hypothalamic (purple) *Lhx6*$^+$ cells at E11.5 and E12.5, with ID (red) and TT (blue) are highlighted in I (E11.5) and J (E12.5). Note anterior domains to the ID that shows a weak and transient *Lhx6* expression during development (Ant.ID = anterior ID, DMH = dorsomedial hypothalamus). (K, L) Distribution of Lhx6$^+$ neurons shown in a sagittal plane using *Lhx6-GFP* transgenic line at postnatal day (P) 49. (M) scRNA-Seq from E11-E13 hypothalamus scRNA-Seq from (D. W. Kim et al., 2019) showing distribution of cells that express GABAergic markers (Blue, *Dlx1/2*, *Gad1/2* and *Slc32a1*) and Lhx6$^+$ GABAergic cells that are ~2% of all hypothalamic GABAergic cells during development. Scale bar = 0.45 mm (A), 0.5 mm (B, G, H), 0.55 mm (C), 0.6 mm (D, K) .

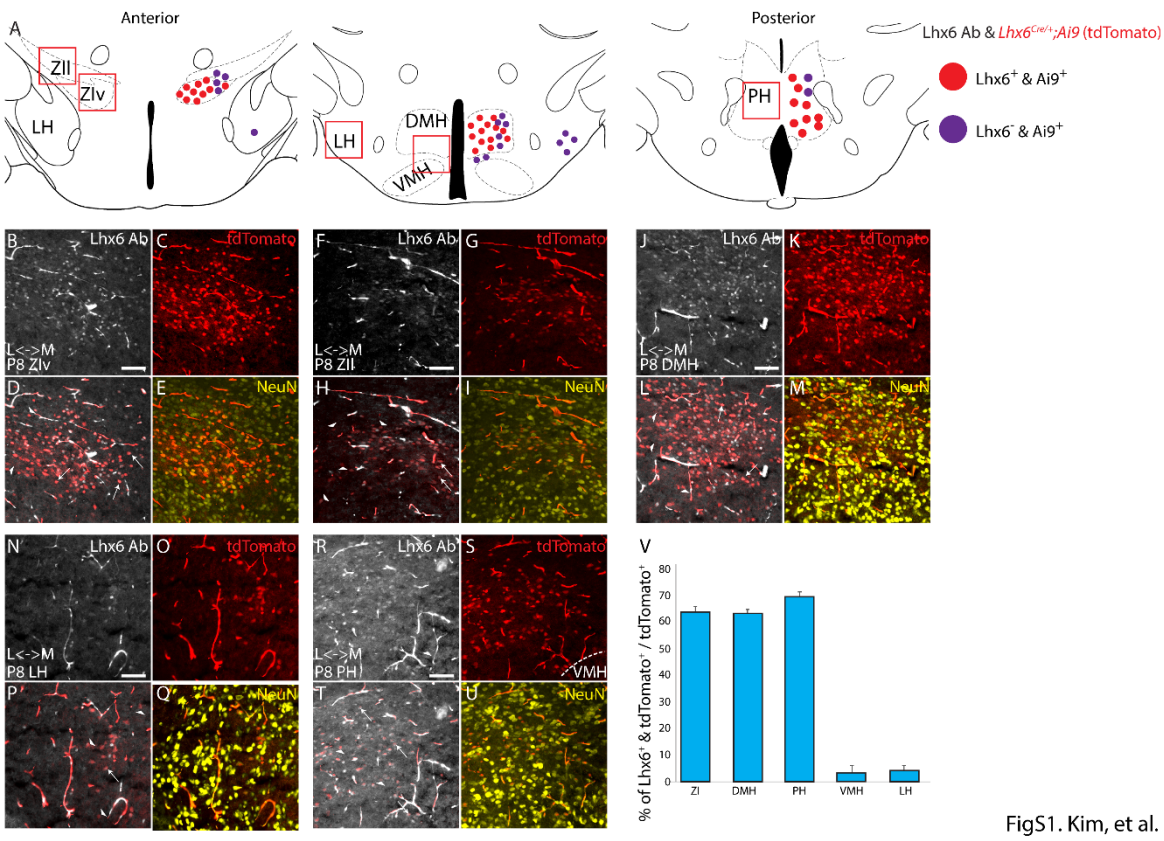

Supplemental figure 1. (A) Schematic distribution of Lhx6^{+} neurons across the dorsolateral hypothalamus (red = neurons that continue to express *Lhx6*, blue = neurons that transiently expressed *Lhx6*) across ZIv (zona incerta ventral), ZII (zona incerta lateral), LH (lateral hypothalamus), DMH (dorsomedial hypothalamus), VMH (ventromedial hypothalamus), PH (posterior hypothalamus). (B-U) Lhx6 antibody staining (grey, B, D, F, H, J, L, N, P, R, T), tdTomato expression from *Lhx6*$^{Cre/+;}$*;Ai9* line (red, C-E, G-I, K-M, O-Q, S-U), NeuN (yellow, E, I, M, Q, U) in ZIv (B-E), ZII (F-L), DMH (J-M), LH (N-Q), PH (R-U). L = lateral, M = medial. (V) Bar graph showing the percentage of tdTomato^{+} and Lhx6^{+} neurons over the total number of tdTomato^{+} neurons.

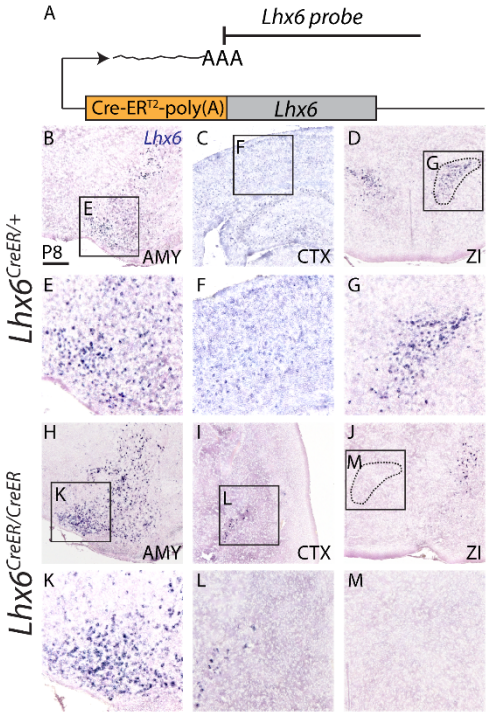

Fig2. Kim, et al.

Figure 2. *Lhx6* mRNA is not detected in Lhx6-deficient hypothalamus, but is detected in telencephalon. (A) *Lhx6*^{CreER} knock-in site (JAX #010776) and location of *Lhx6* probe used to detect read-through transcription. (B-M) Coronal planes showing *Lhx6* mRNA expression in amygdala (AMY, B, E, H, K), cortex (CTX, C, F, I, L), and zona incerta (ZI, D, G, J, M) in control (*Lhx6*$^{CreER/+}$, B-G) and mutant (*Lhx6*$^{CreER/CreER}$, H-M) at P8. Note the absence of Lhx6 mRNA in mutant ZI (J, M). Scale bar = 0.6 mm.

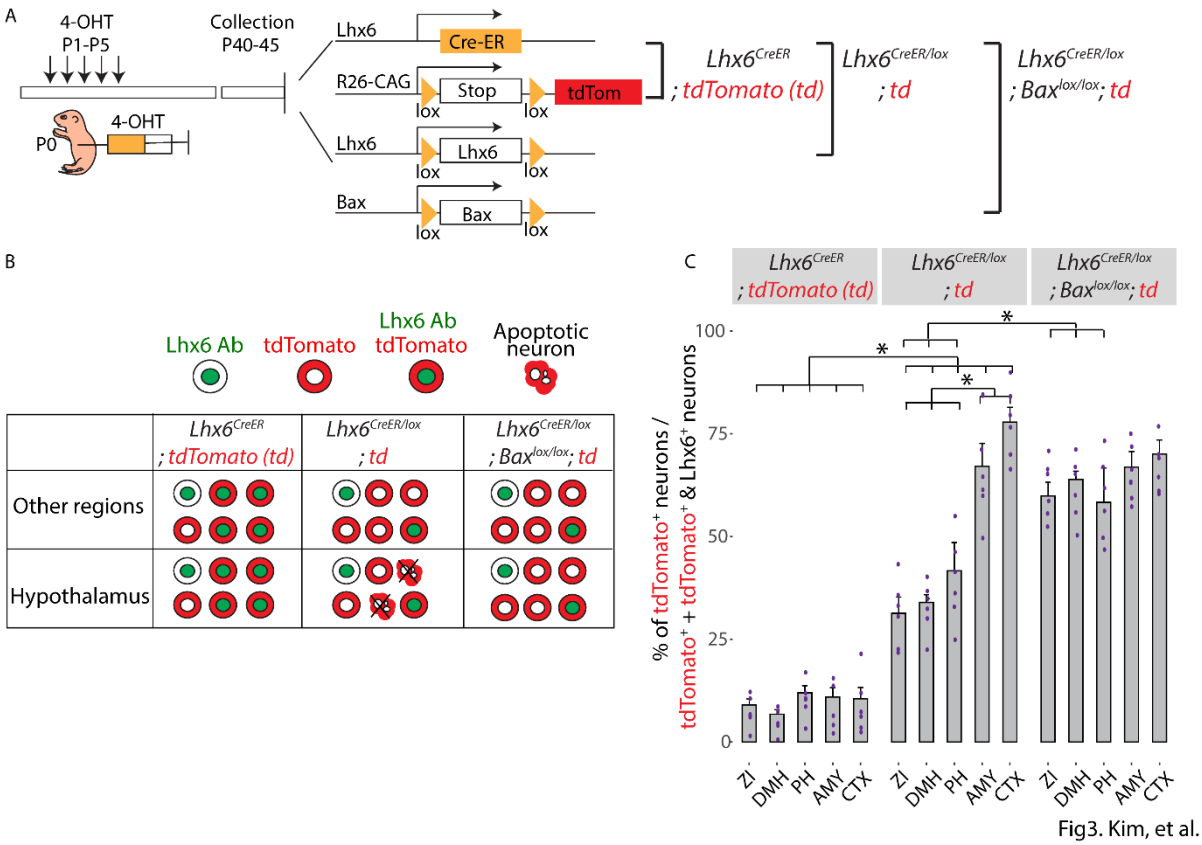

Figure 3. Hypothalamic *Lhx6* is important for cell survival. (A) Schematic diagram showing the overall design of the experiment from 3 genotypes (1. *Lhx6*$^{CreER/+}$*;Ai9*, 2. *Lhx6*$^{CreER/+}$*; Lhx6*$^{lox/+}$*;Ai9*, 3. *Lhx6*$^{CreER/+}$*;Lhx6*$^{lox/+}$*;Bax*$^{lox/lox}$*;Ai9*). (B) Schematic diagram showing the overall outcome of the experiment. (C) A bar graph showing the percentage of tdTomato^{+} / (tdTomato^{+} & tdTomato^{+}/Lhx6^{+}) across 3 genotypes in 5 different brain regions. * indicates $p < 0.05$. ZI = zona incerta, DMH = dorsomedial hypothalamus, PH = posterior hypothalamus, AMY = amygdala, CTX = cortex.

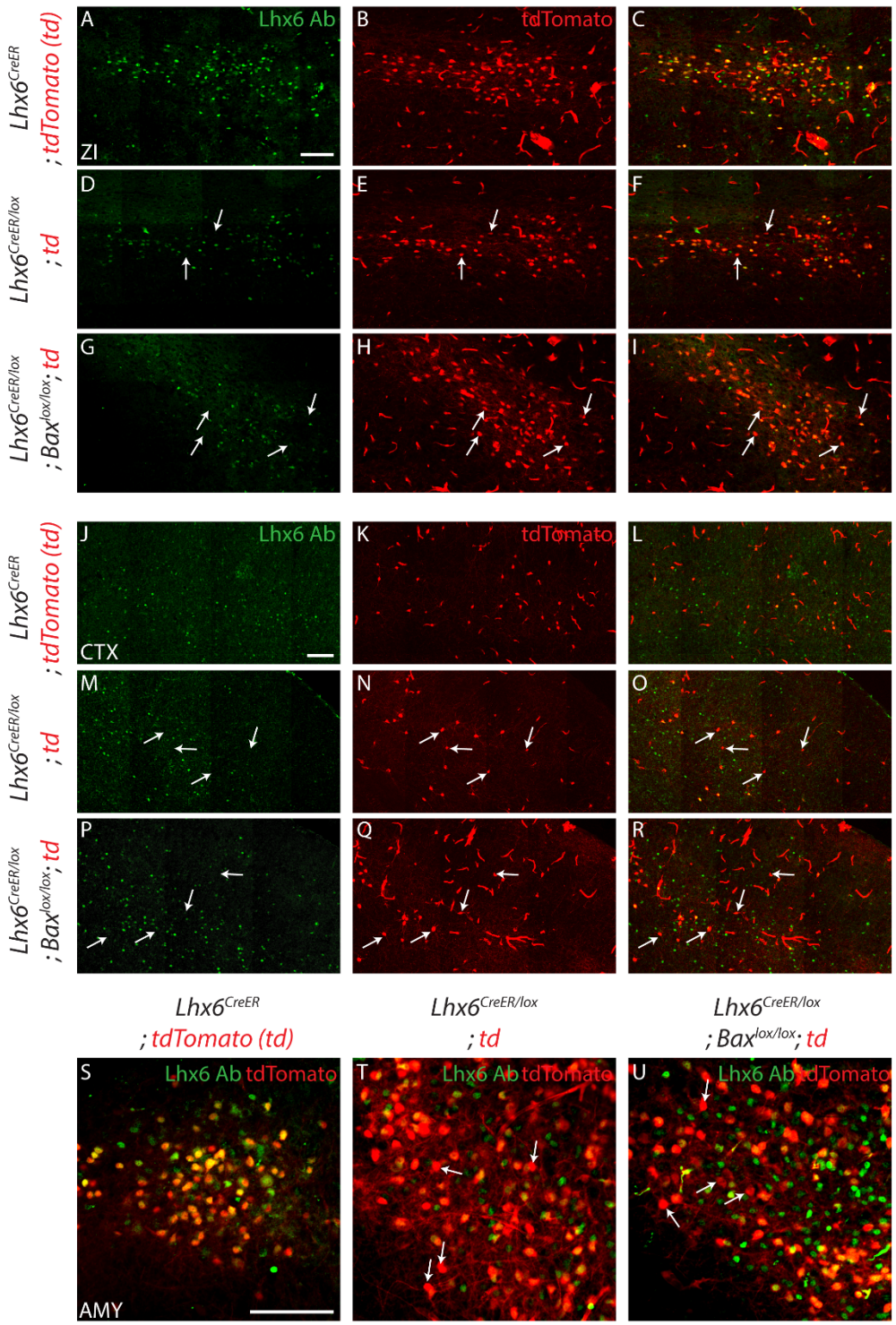

FigS2. Kim, et al.

Supplemental figure 2. Representative images of 3 genotypes (1. *Lhx6*$^{CreER/+}$*;Ai9* (A-C, J-L, S), 2. *Lhx6*$^{CreER/+}$*; Lhx6*$^{lox/+}$*;Ai9* (D-F, M-O, T), 3. *Lhx6*$^{CreER/+}$*;Lhx6*$^{lox/+}$*;Bax*$^{lox/lox}$*;Ai9* (G-I, P-R, U)) in zona incerta (ZI, A-I), cortex (CTX, J-R), and amygdala (AMY, S-U) with tdTomato (red) and Lhx6 antibody staining (Lhx6 Ab, green). White indicates tdTomato^{+} cells without Lhx6 expression. Scale bar = 100 μm. 4-OHT was administered between P1 and P5, and animals were collected between P40 and P45.

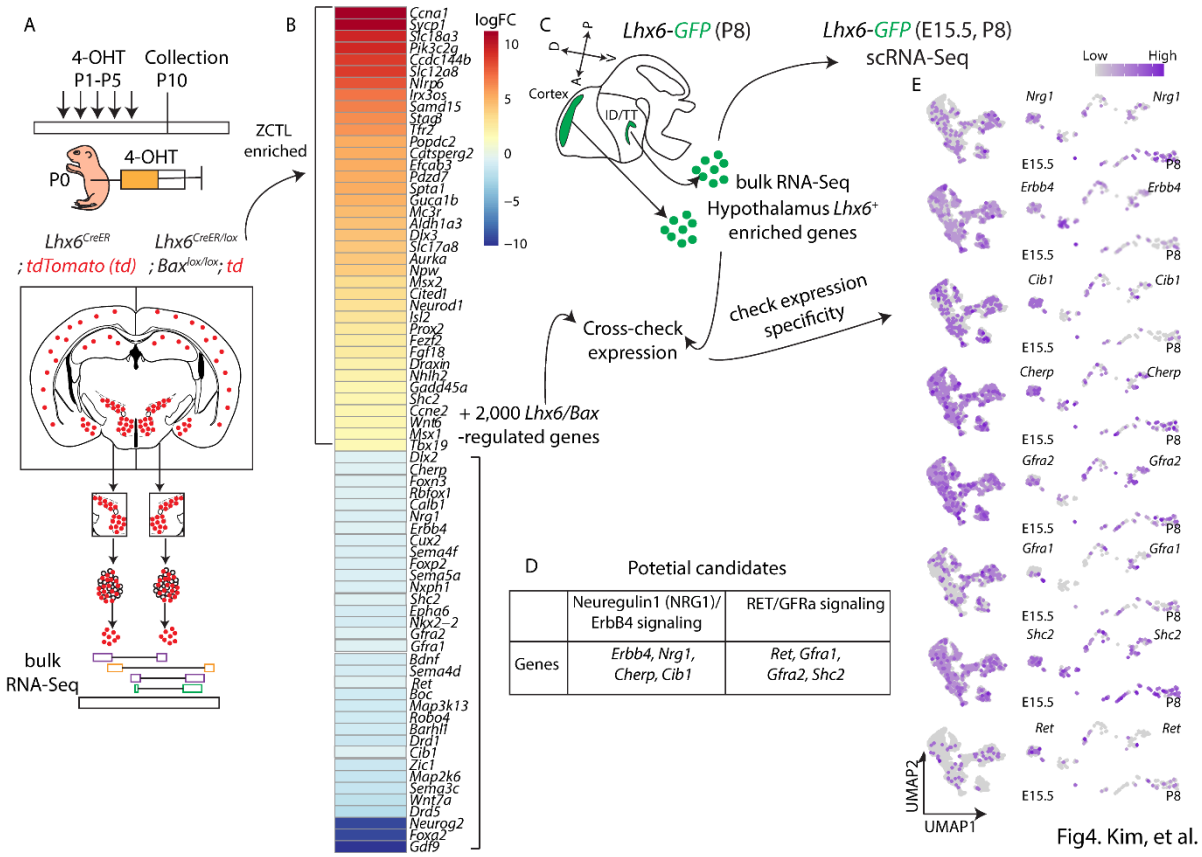

Figure 4. Potential candidates that can regulate survival in hypothalamic Lhx6⁺ cells. (A) Schematic showing bulk RNA-Seq pipeline from *Lhx6*$^{CreER/+}$*;Ai9* and *Lhx6*$^{CreER/+}$*;Lhx6*$^{lox/+}$*;Bax*$^{lox/lox}$*;Ai9*. (B) Heatmap showing examples of genes (full list in Table. S1) that are enriched in *Lhx6*$^{CreER/+}$*;Ai9* or *Lhx6*$^{CreER/+}$*;Lhx6*$^{lox/+}$*;Bax*$^{lox/lox}$*;Ai9*. Note upregulation of genes that are involved in cell proliferation (*Ccna1, Aurka*) and neural precursor cells (*Irx3os, Cited1, Neurod1*). (C) Schematic showing bulk RNA-Seq from P8 *Lhx6-GFP* cortex and hypothalamus, and scRNA-Seq from E15 and P8 *Lhx6-GFP* hypothalamus. (D) Potential candidate genes controlling cell survival can be regulated by *Lhx6* in hypothalamic Lhx6⁺ cells - Neuregulin-ErbB4 signaling and Gdnf signaling pathways. (E) UMAP plots showing thatgenes in D are robustly expressed in E15 and P8 hypothalamus Lhx6⁺ cells from the *Lhx6-GFP* scRNA-Seq dataset.

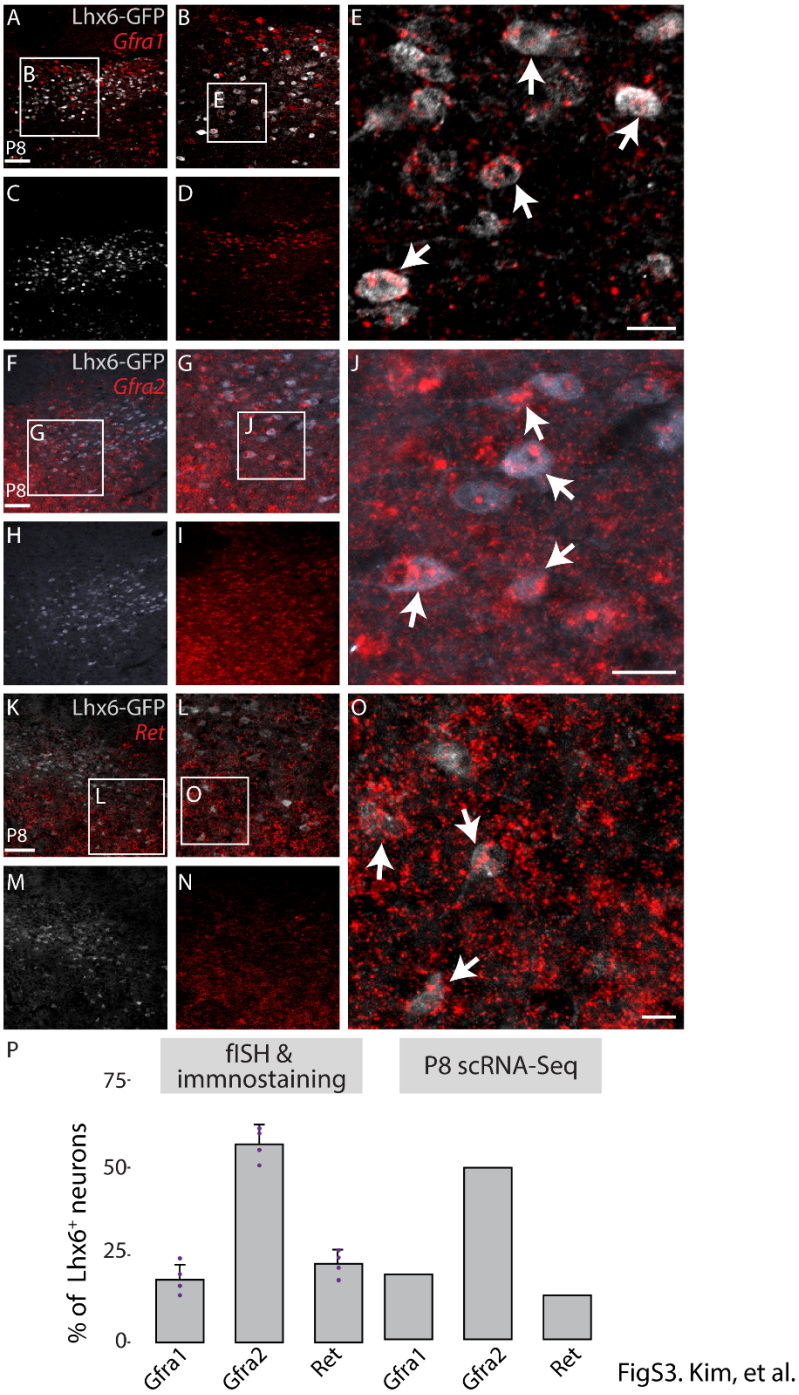

Supplemental figure 3. Representative images of *Gfra1* (red, A-E), *Gfra2* (red, F-J), *Ret* (red, K-O) in Lhx6$^+$ cells at P8 in the *Lhx6-GFP* line (grey). White arrows in E, J, O show GFP$^+$ and *Gfra1*$^+$ (E,), *Gfra2*$^+$ (J), *Ret*$^+$ (O). Scale bar = 100 µm (A, F, K), 15 µm (E, J, O). (P) Bar graph showing the percentage of *Gfra1*$^+$/*Gfra2*$^+$/*Ret*$^+$ Lhx6$^+$ cells from 1) fISH (*Gfra1/Gfra2/Ret*, Red) and immunostaining of GFP in *Lhx6-GFP* line (grey) (left), and 2) P8 scRNA-Seq data from flow-sorted hypothalamic GFP$^+$ cells from *Lhx6-GFP* mice (right).

Table S1. Differential gene lists from bulk RNA-Seq between *Lhx6*$^{CreER/+}$*;Ai9* and *Lhx6*$^{CreER/+}$*;Lhx6*$^{lox/+}$*;Bax*$^{lox/lox}$*;Ai9***.**

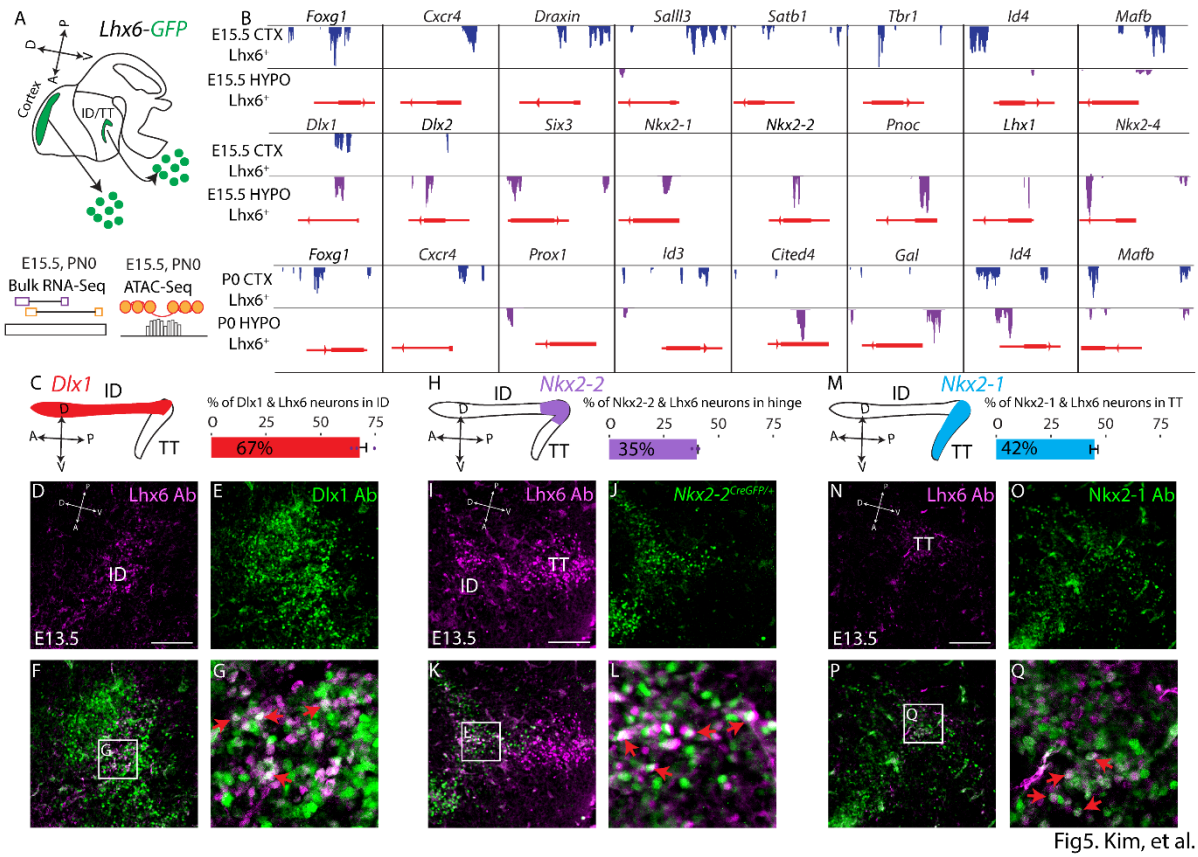

Figure 5. Molecular markers demonstrate that hypothalamic Lhx6 cells are organized into distinct spatial domains. (A) Schematic showing bulk RNA-Seq and bulk ATAC-Seq pipelines from flow-sorted *Lhx6-GFP*$^{+}$ cells of the cortex and hypothalamus at E15.5 and P0. (B) ATAC-Seq footprinting showing potential transcription factor binding sites near the promoter regions of differentially expressed genes from bulk RNA-Seq data in the cortex and hypothalamus at E15.5 and P0 (C) Schematic showing the ID/TT of the developing hypothalamus and expression of *Dlx1/2* (left), and the percentage of ID Lhx6+ cells that co-express *Dlx1* (right). (E-G) Immunostaining with Lhx6 (D, F, G) and Dlx1 (E, F, G) of E13 hypothalamus, showing co-localization of Lhx6 and Dlx1 in ID of the hypothalamus (G, red arrows). Scale bar = 50 µm. (H) Schematic showing ID/TT of the developing hypothalamus and expression of *Nkx2-2* (left) and the percentage of hinge Lhx6+ cells that co-express *Nkx2-2* (right). (I-L) Immunostaining with Lhx6 (I, K, L) and GFP in *Nkx2-2*$^{CreGFP/+}$ (J, K, L) of E13 hypothalamus show co-localization of Lhx6 and *Nkx2-2*^{GFP} between ID and TT (hinge region) of the hypothalamus (L, red arrows). Scale bar = 50 µm. (M) Schematic showing ID/TT of the developing hypothalamus and expression of *Nkx2-1* (left) and the percentage TT Lhx6+ cells that co-express *Nkx2-1* (right). (N-Q) Immunostaining with Lhx6 (N, P, Q) and Nkx2-1 (O, P, Q) of E13 hypothalamus, showing co-localization of Lhx6 and Dlx1 in ID of the hypothalamus (Q, red arrows). Scale bar = 50 µm.

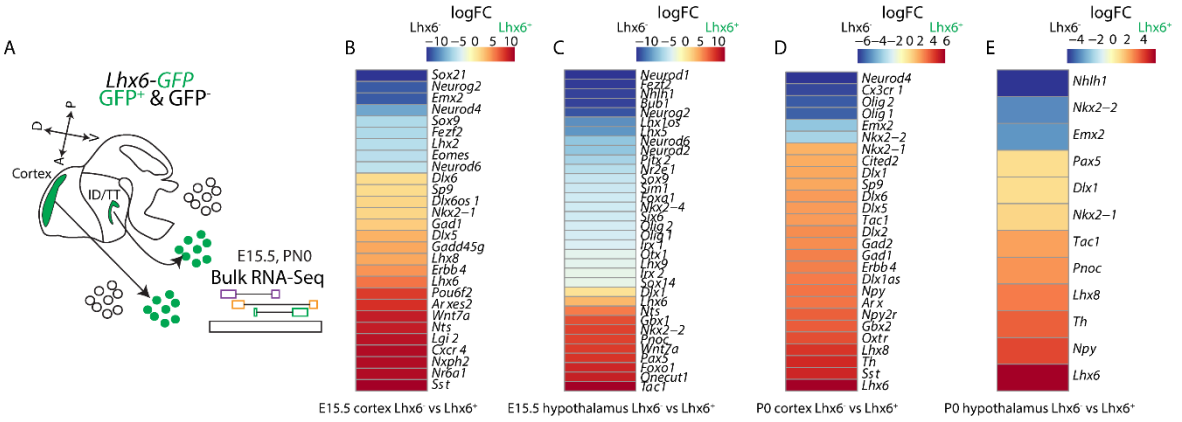

FigS4. Kim, et al.

Supplemental figure 4. Heatmap showing examples of genes (full list in Table. S3) that are enriched in *Lhx6-GFP*$^{+}$ cells compared to *Lhx6-GFP*$^{-}$ cells of the cortex and hypothalamus at E15.5 and P0.

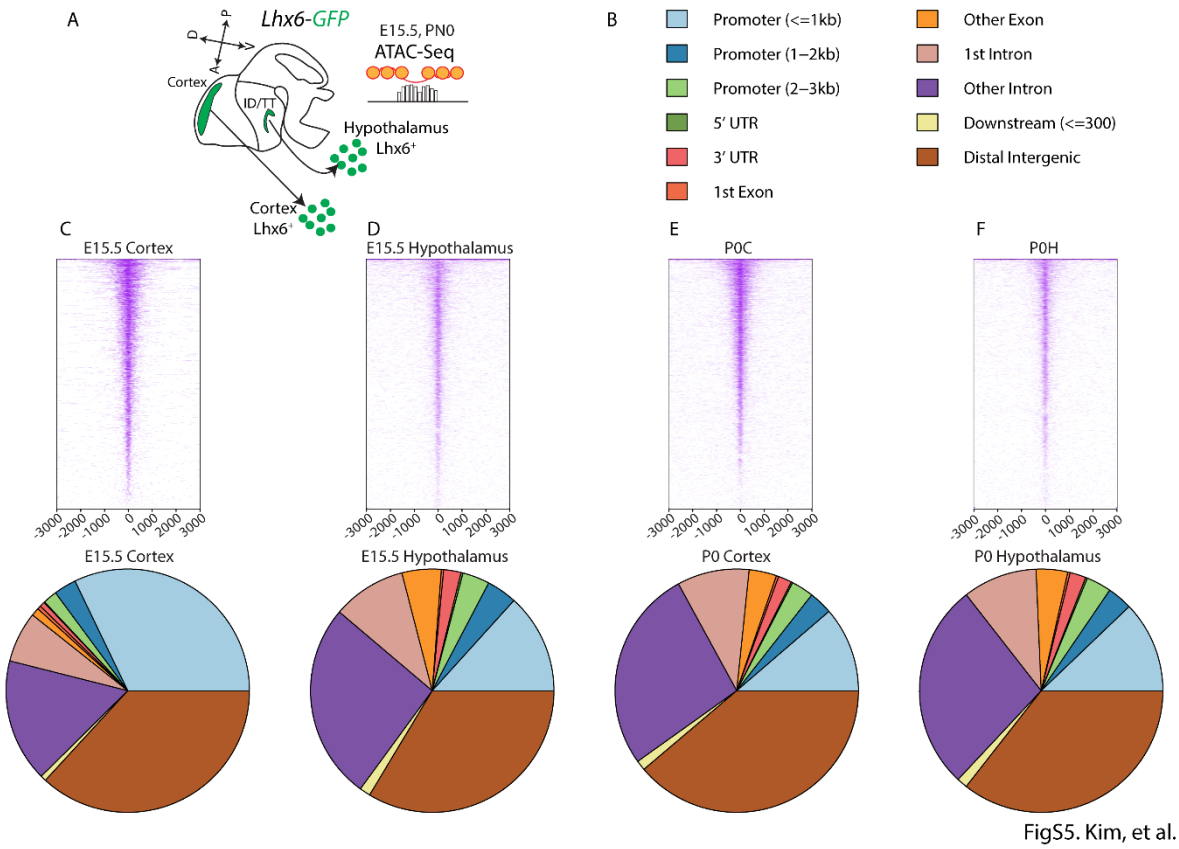

Supplemental figure 5. (A) Schematic showing bulk ATAC-Seq pipeline from flow-sorted *Lhx6-GFP*$^{+}$ cells of the cortex and hypothalamus at E15.5 and P0. (B) Legends for pie graphs in (C-F). (C-F) Heatmap showing open chromatic regions (top) in E15.5 (C, D), P0 (E, F), cortex (C, E), hypothalamus (D, F), with distribution of open chromatin regions (pie graphs, bottom).

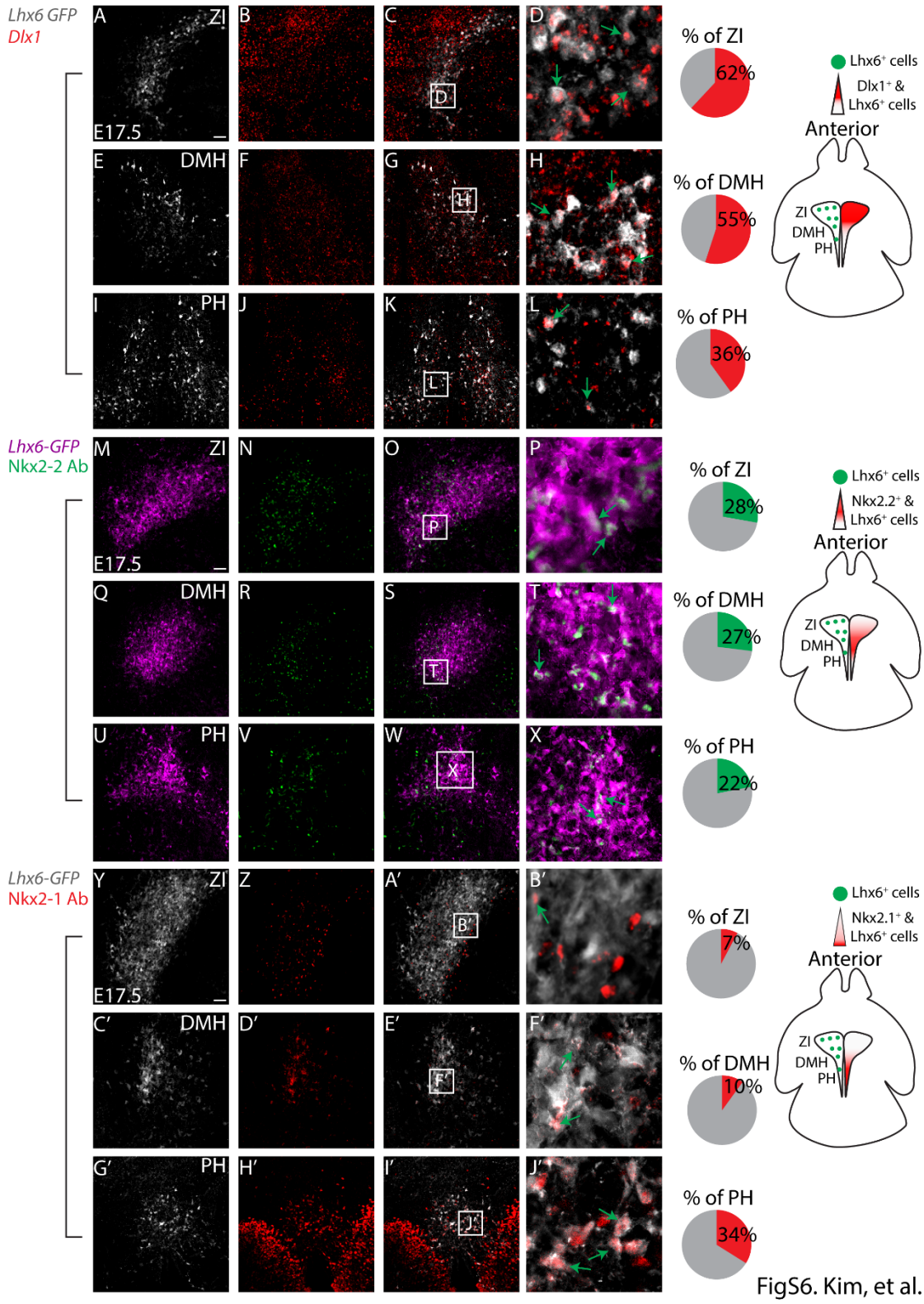

Supplemental figure 6. Staining showing distribution and the percentage of *Dlx1* (A-L *Lhx6-GFP* in grey, *Dlx1* in red), *Nkx2-2* (M-X, *Lhx6-GFP* in magenta, Nkx2-2 in green), and *Nkx2-1* (Y-J', *Lhx6-GFP* in grey, Nkx2-1 in red) in E17 zona incerta (ZI, A-D, M-P, Y-B'), dorsomedial hypothalamus (DMH, E-H, Q-T, C'-F'), and posterior hypothalamus (PH, I-L, U-X, G'-J'). Scale bar = 50 μm.

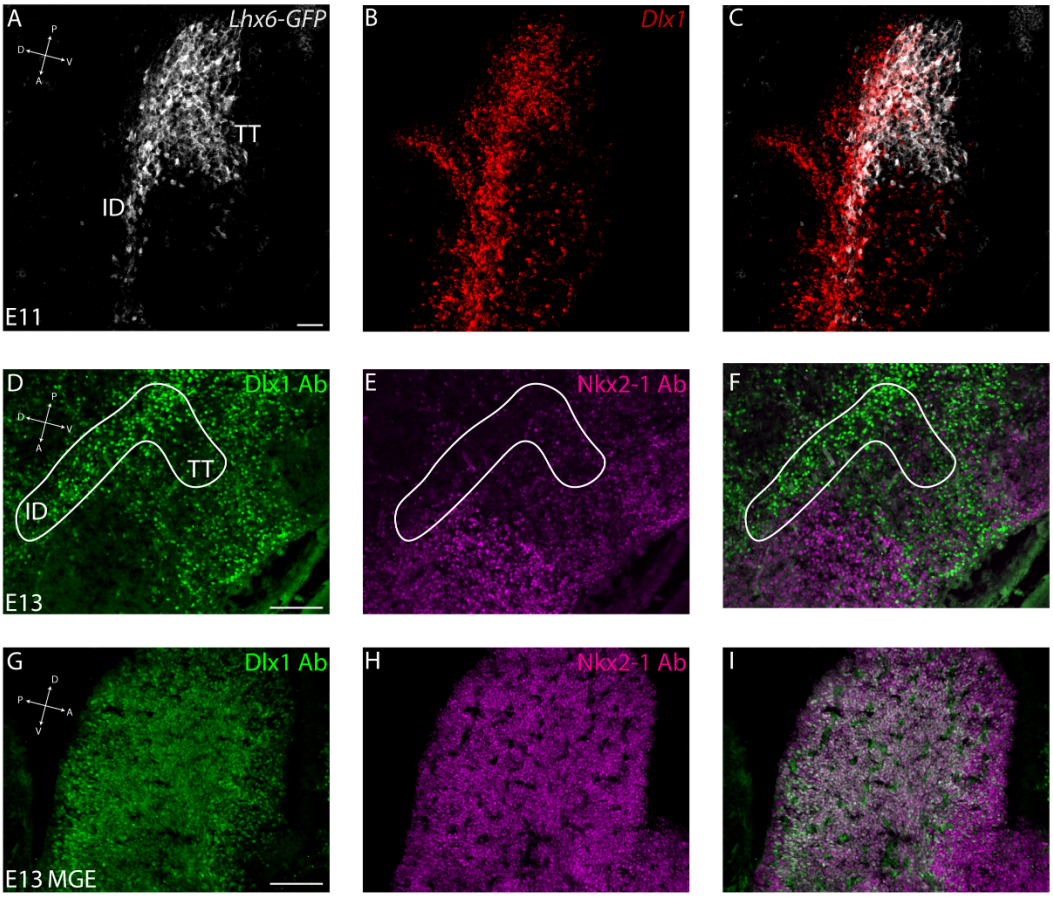

FigS7. Kim, et al.

Supplemental figure 7. Dlx1/2 and Nkx2-1 expression delineates separate zones in the ID and TT. (A-C) fISH showing GFP expression in *Lhx6-GFP* line at E11 (A, C, grey) and *Dlx1* (B-C, red). Note *Dlx1* covers most of the ID. (D-F) Immunostaining of Dlx1 (D, F, green) and Nkx2-1 (E, F, magenta) in E13 ID and TT. Note the lack of co-expression Dlx1 and Nkx2-1. (G-I) Immunostaining of Dlx1 (G, I, green) and Nkx2-1 (H, I magenta) in E13 MGE. Note high level of co-expression Dlx1 and Nkx2-1. Scale bar = 50 μm.

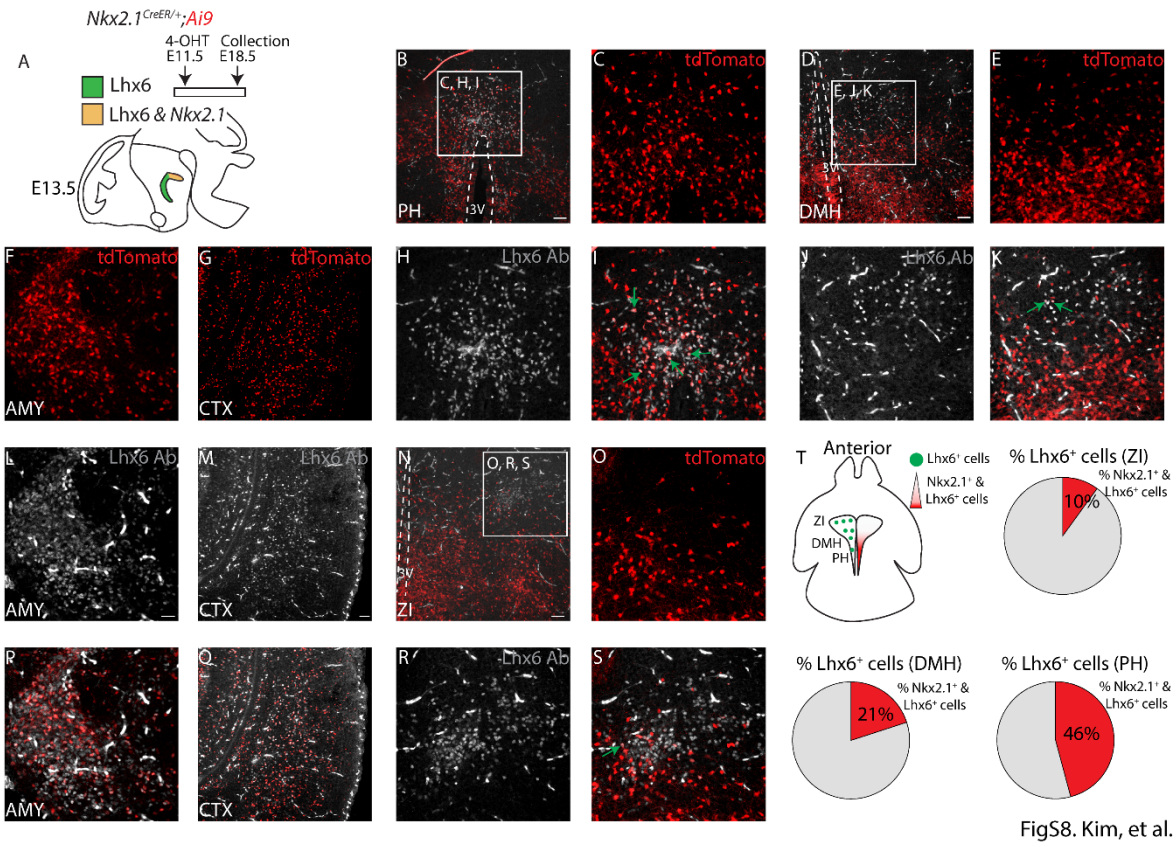

Supplemental figure 8. Nkx2-1 is required only for specification of posterior hypothalamic Lhx6$^+$ neurons. (A) Schematic showing 4-OHT treatment into E11 *Nkx2-1$^{CreER/+;}$Ai9* dams and collection of embryos at E18.5 (top), and schematic showing distribution of *Nkx2-1$^-$/Lhx6$^+$* in ID (anterior) and *Nkx2-1$^+$/Lhx6$^+$* in TT (posterior). (B-S) Immunostaining showing Lhx6 (grey, B, D, H, I, J, K, L, M, N, P, Q, R, S) and tdTomato (red, *Nkx2-1$^{CreER/+;}$Ai9*, B, C, D, E, F, G, I, K, N, O, P, Q, S) in amygdala (AMY, F, L, P), cortex (CTX, G, M, Q), posterior hypothalamus (PH, B, C, H, I), dorsomedial hypothalamus (DMH, D, E, J, K), and zona incerta (ZI, N, O, R, ST). Green arrows show co-localization. (T) Schematic showing horizontal mouse brain section highlighting ZI, DMH, PH, and distribution of hypothalamic Lhx6$^+$ cells and Nkx2-1$^+$/Lhx6$^+$ cells are shown (top left). Pie graphs showing the percentage of Nkx2-1$^+$/Lhx6$^+$ cells. Note a posterior bias in distribution of Nkx2-1$^+$/Lhx6$^+$ cells. Scale bar = 50 µm.

Table S2. Differential gene lists from bulk RNA-Seq between cortical and hypothalamic *Lhx6-GFP$^+$* cells at E15.5 and P0.

Table S3. Differential gene lists from bulk RNA-Seq between *Lhx6-GFP$^+$* and *Lhx6-GFP$^-$* cells of cortex and hypothalamus at E15.5 and P0.

Table S4. Differential peaks from ATAC-Seq between cortical and hypothalamic *Lhx6-GFP$^+$* cells at E15.5.

Table S5. Differential peaks from ATAC-Seq between cortical and hypothalamic *Lhx6-GFP$^+$* cells at P0.

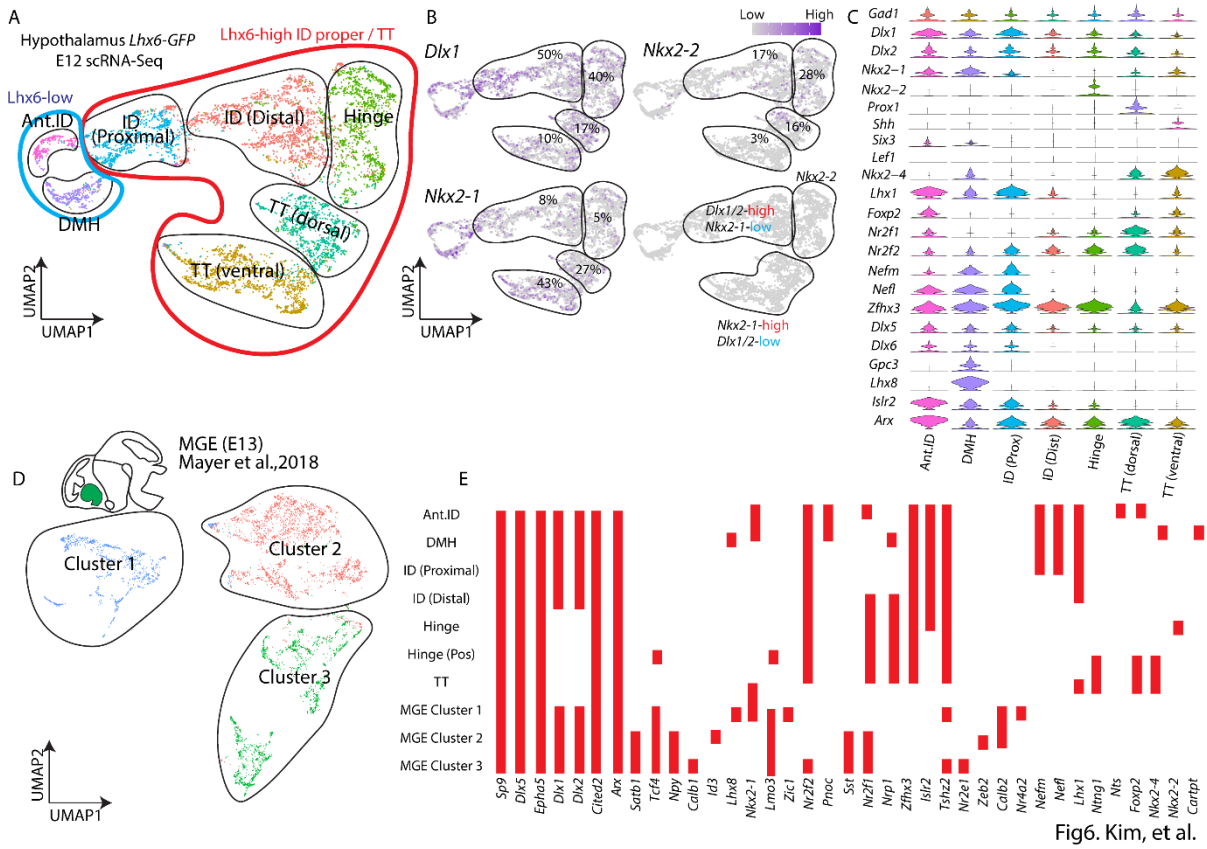

Figure 6. ScRNA-Seq identifies molecular markers of spatially distinct domains of hypothalamic Lhx6 neurons. (A) UMAP plot showing different Lhx6^{+} hypothalamic regions at E12.5. (B) UMAP plots showing expression and percentage of ID, hinge, TT, expressing *Dlx1/2* , *Nkx2-2*, and *Nkx2-1*. (C) Violin plots showing expression of key transcription factors (and other genes) that are highly expressed in individual domains. (D) UMAP plot showing different Lhx6^{+} medial ganglionic eminence (MGE) regions at E13.5. Data from (Mayer et al., 2018). (E) Graph showing presence (red bar) of key genes that are expressed in hypothalamic and/or MGE LHx6^{+} populations. Note lack of overlap in gene expression profiles between hypothalamus MGE Lhx6^{+} populations. Ant.ID = anterior ID, DMH = dorsomedial hypothalamus.

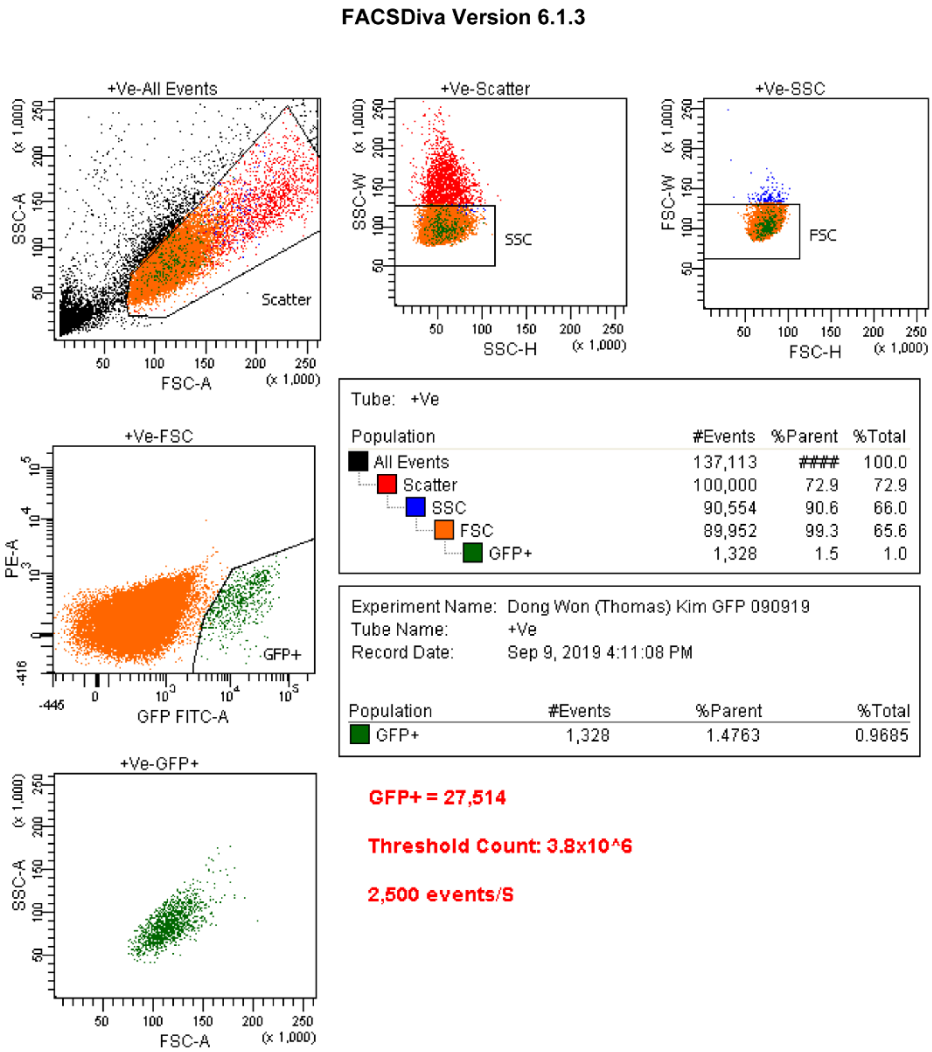

FigS9. Kim, et al.

Supplemental figure 9. Flow-sorting data for isolated GFP^{+} cells in *Lhx6-GFP* line.

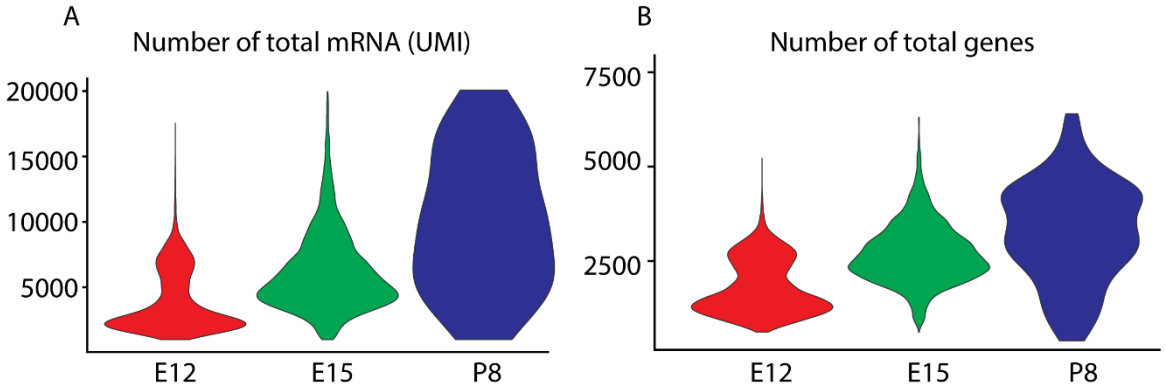

FigS10. Kim, et al.

Supplemental figure 10. Violin plots showing the number of total mRNAs (A) and number of total genes (B) in E12.5, E15.5, and P8 *Lhx6-GFP* scRNA-Seq.

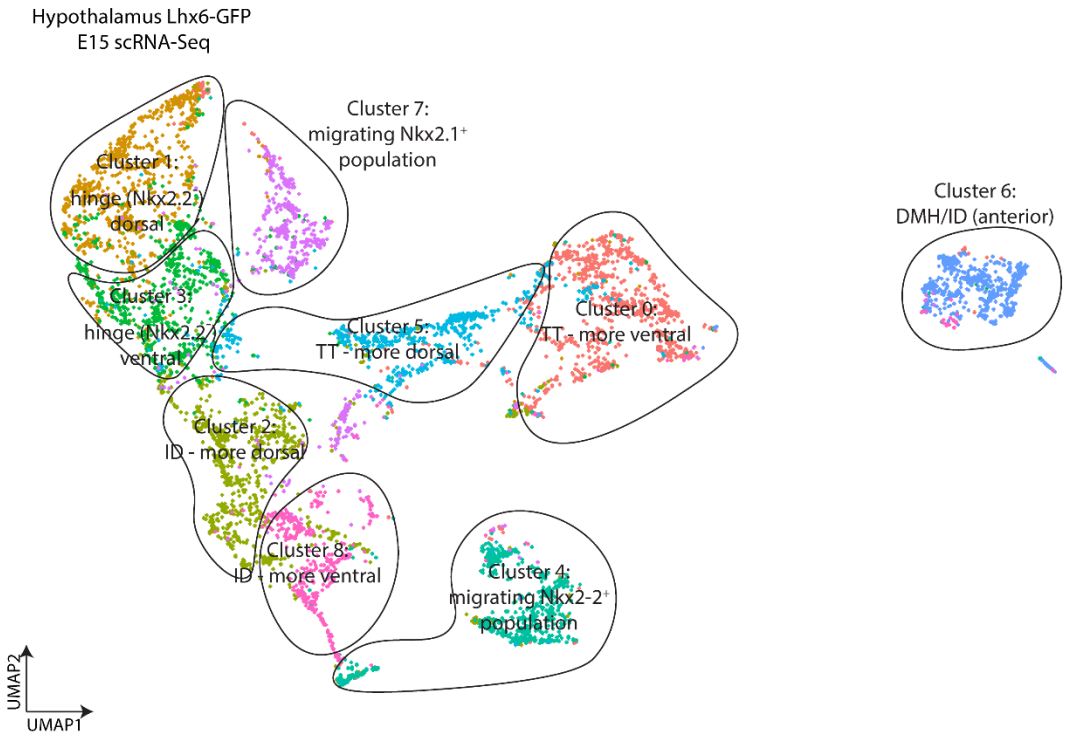

FigS11. Kim, et al.

Supplemental figure 11. scRNA-Seq captures molecularly diverse hypothalamic Lhx6$^+$ domains at E15.5.

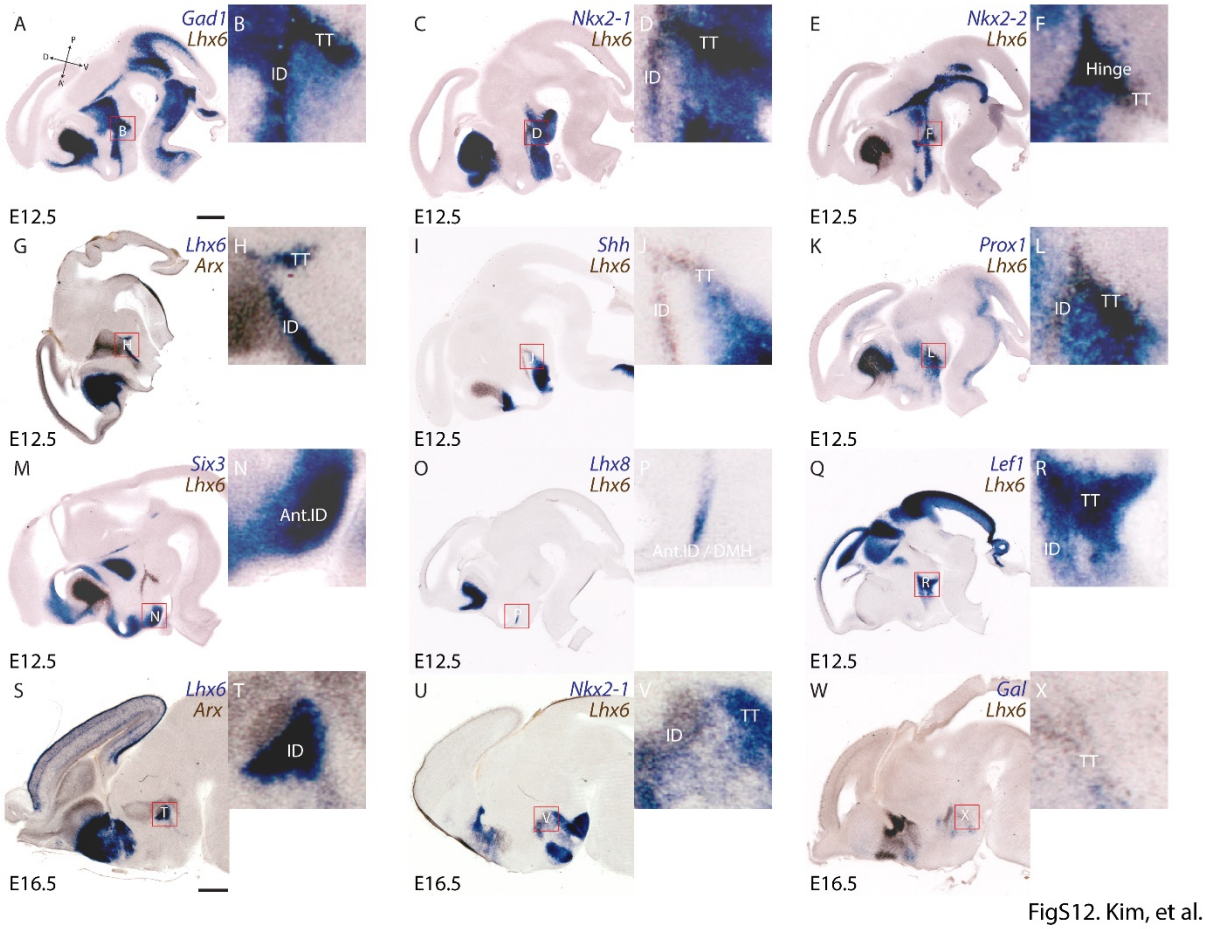

Supplemental figure 12. *In situ* hybridization showing *Lhx6* with *Gad1* (A,B), *Nkx2-1* (C,D,U,V), *Nkx2-2* (E,F), *Arx* (G,H,S,T), *Shh* (I,J), *Prox1* (K,L), *Six3* (M,N), *Lhx8* (O,P), *Lef1* (Q,R), *Gal* (W,X) at E12.5 (A-R) and E16.5 (S-X), shown in sagittal planes. Scale bar = 0.45 mm (A-R), 0.6 mm (S-X) .

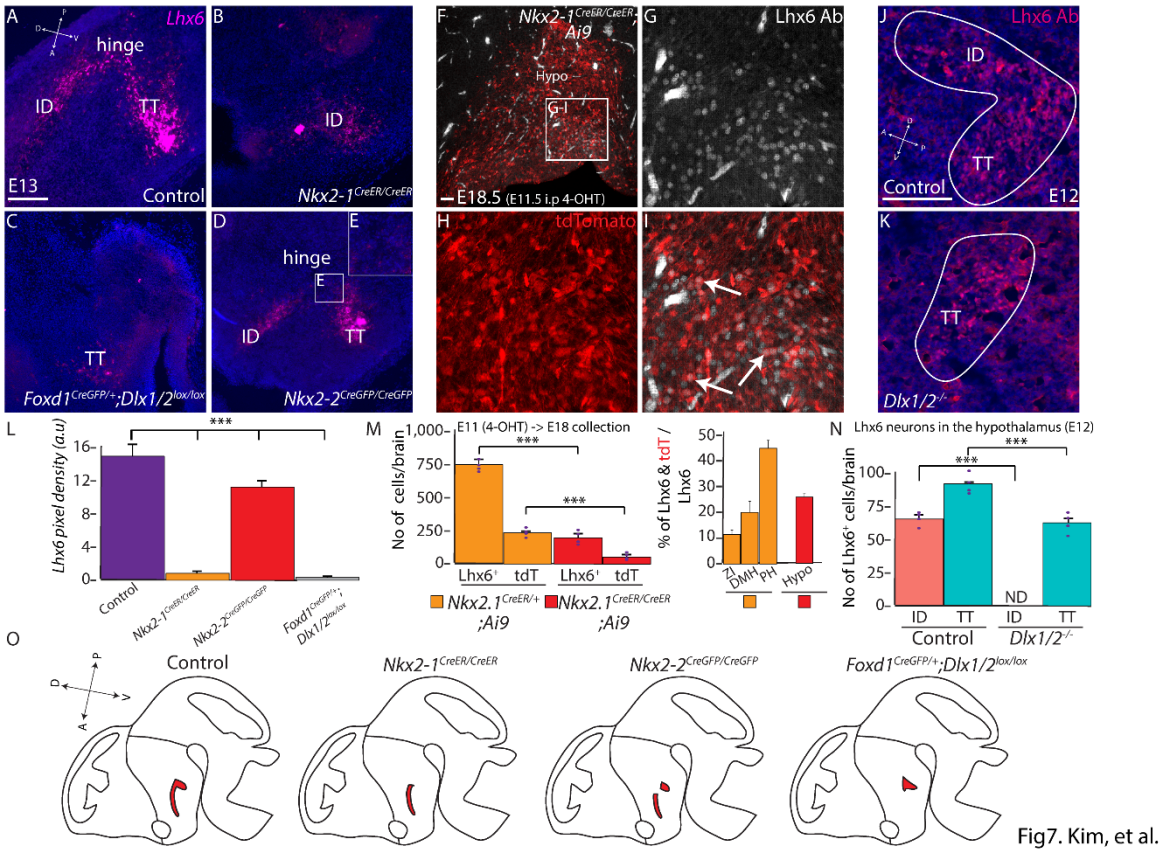

Figure 7. Transcription factor-mediated patterning of discrete spatial domains of hypothalamic Lhx6 neurons. (A-E, L) RNAscope showing *Lhx6* expression (magenta) in control (A), *Nkx2-1*$^{CreER/CreER}$ (B), *Foxd1*$^{Cre/+}$*:Dlx1/2*$^{lox/lox}$ (C), and *Nkx2-2*$^{CreGFP/CreGFP}$ (D-E). Pixel density of *Lhx6* is shown across all 4 groups in (L). (F-I, M) *Nkx2-1*$^{CreER/CreER;}$*Ai9* (4-OHT treatment at E11.5, collection at E18.5) showing Lhx6 expression (grey, G) and tdTomato (red, H) in the hypothalamus. Arrows in I indicate Lhx6^{+} and tdTomato^{+} cells. Raw number of Lhx6^{+} or tdTomato^{+} (tdT) cells (left) and percentage of Lhx6^{+} & tdTomato^{+} cells (right) in *Nkx2-1*$^{CreER/+}$*;Ai9* (Fig. S5) and *Nkx2-1*$^{CreER/CreER}$*/Ai9*. (J-K, N) Lhx6 expression (magenta) in control and Dlx1/2$^{-/-}$ at E12 ID and TT. Number of Lhx6^{+} cells in ID and TT are shown in (N). (O) Schematic diagram showing distribution of *Lhx6* expression across 4 groups. ID = intrahypothalamic diagonal, TT = tuberomamillary terminal. Scale bar = 50 µm. *** $p < 0.05$.

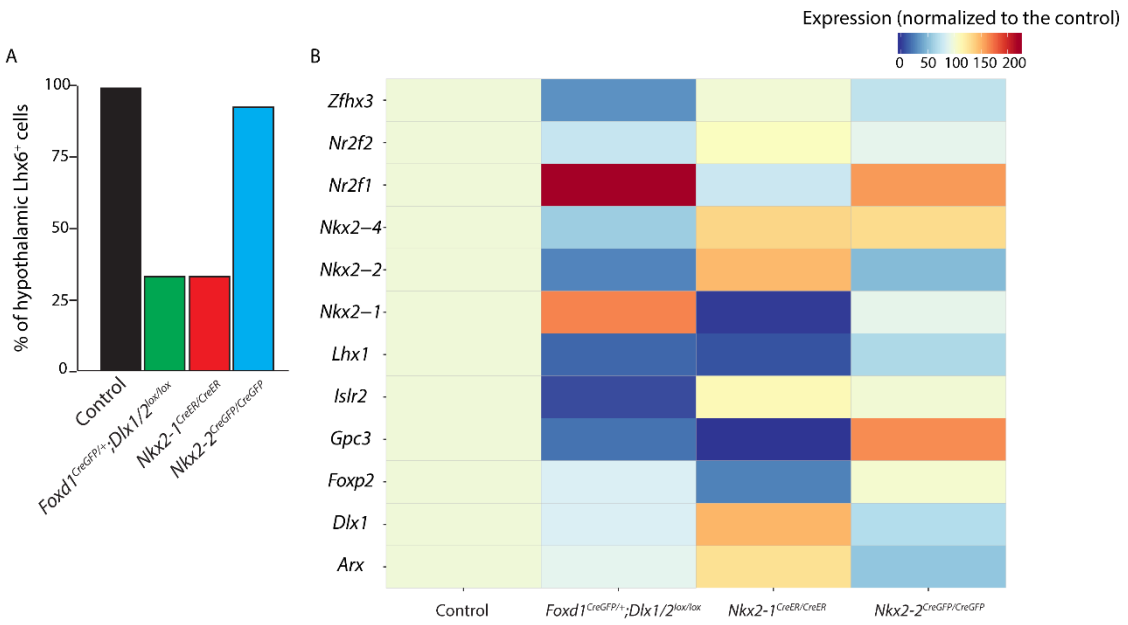

FigS13. Kim, et al.

Supplemental figure 13. scRNA-Seq result from (D. W. Kim et al., 2019), *Foxd1*$^{Cre/+}$*;Dlx1/2*$^{lox/lox}$*, Nkx2-1*$^{CreER/CreER}$*, Nkx2-2*$^{CreGFP/CreGFP}$ from hypothalamic *Lhx6*$^{+}$ cells. (A) Bar graph showing the percentage of cells that express *Lhx6* across 4 genotypes. (B) Heatmap showing changes in percentage of transcription factors across 4 genotypes.

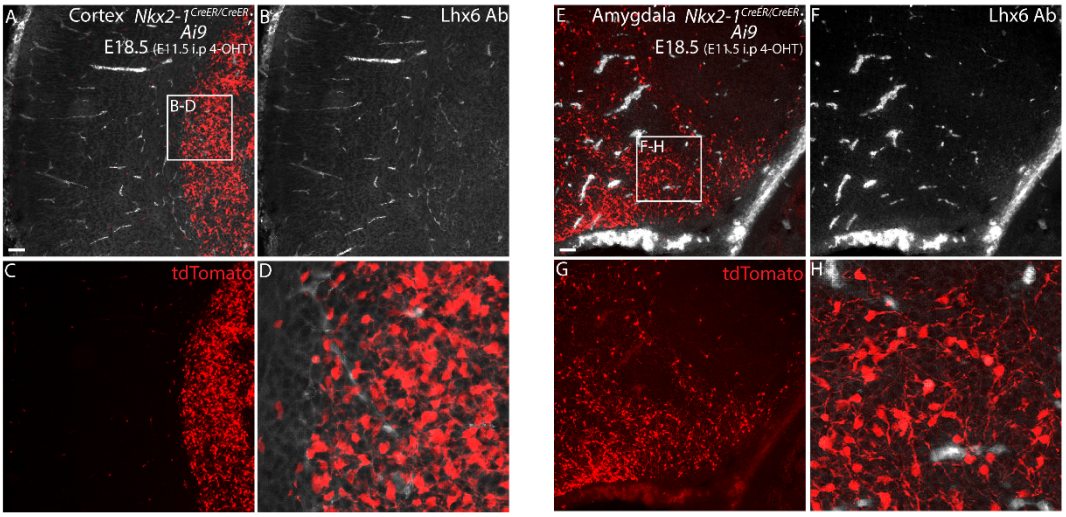

FigS14. Kim, et al.

Supplemental figure 14. *Nkx2-1*$^{CreER/CreER;}$*Ai9* (4-OHT treatment at E11.5, collection at E18.5) showing Lhx6 expression (grey, A, B, D, E, F, H) and tdTomato (red, A, C, D, E, G, H) in the cortex (A-D) and amygdala (E-H). Note the absence of Lhx6^{+} cells in both brain regions. Scale bar = 50 µm.

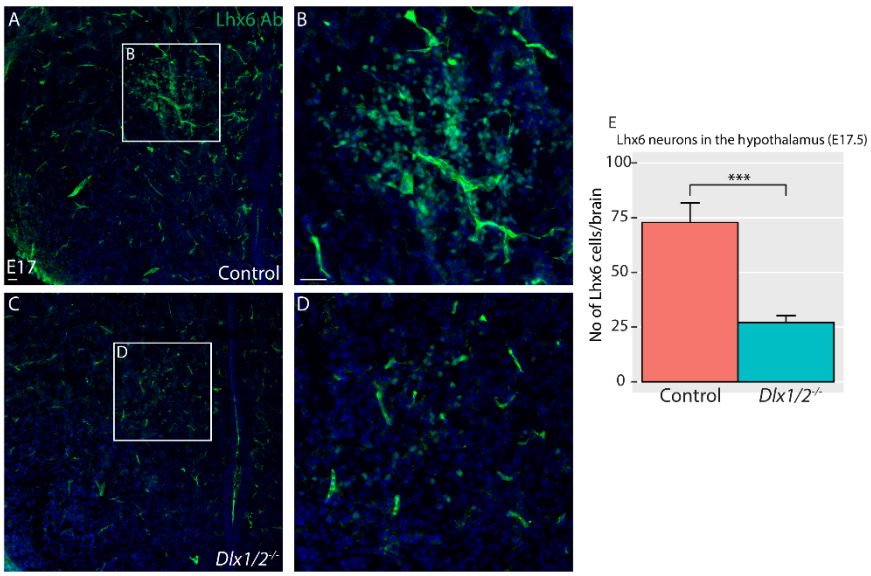

FigS15. Kim, et al.

Supplemental figure 15. Lhx6 expression (green) in control (A, B) and Dlx1/2$^{-/-}$ (C,D) at E17 ZI. Number of Lhx6^{+} cells are shown in (E). ZI = zona incerta. Scale bar = 50 µm. *** $p < 0.05$

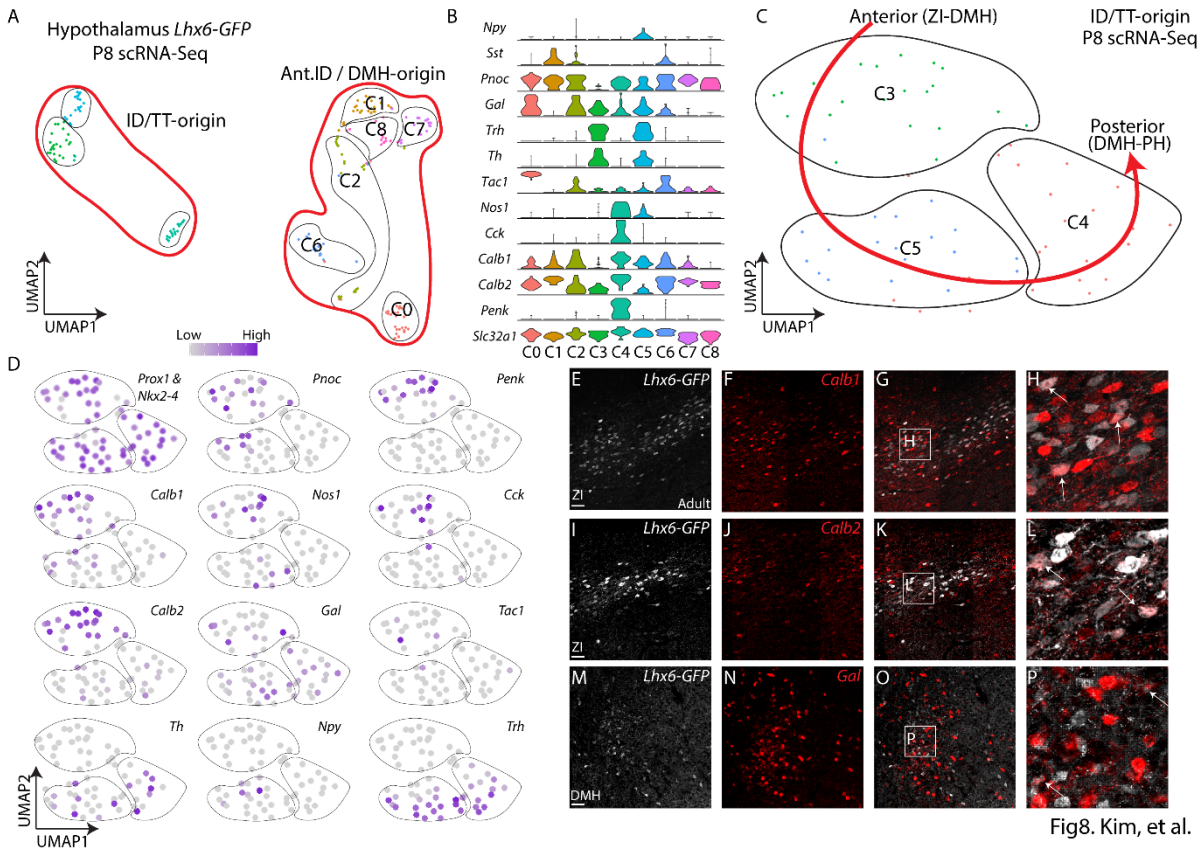

Figure 8. (A) UMAP plot showing hypothalamic Lhx6$^+$ GABAergic neurons at P8. (B) Violin plots showing key markers in individual clusters in A. (C) UMAP plot showing Lhx6$^+$ cells originated from ID and TT. (D) UMAP plots showing distribution of diverse neuropeptides and neurotransmitters across ID and TT derived Lhx6$^+$ neurons. (E-P) Fluorescent *in situ* hybridization showing *Lhx6-GFP* (grey) with *Calb1* (red, E-H), *Calb2* (red, I-L), and *Gal* (red, M-P). Scale bar = 50 μm.

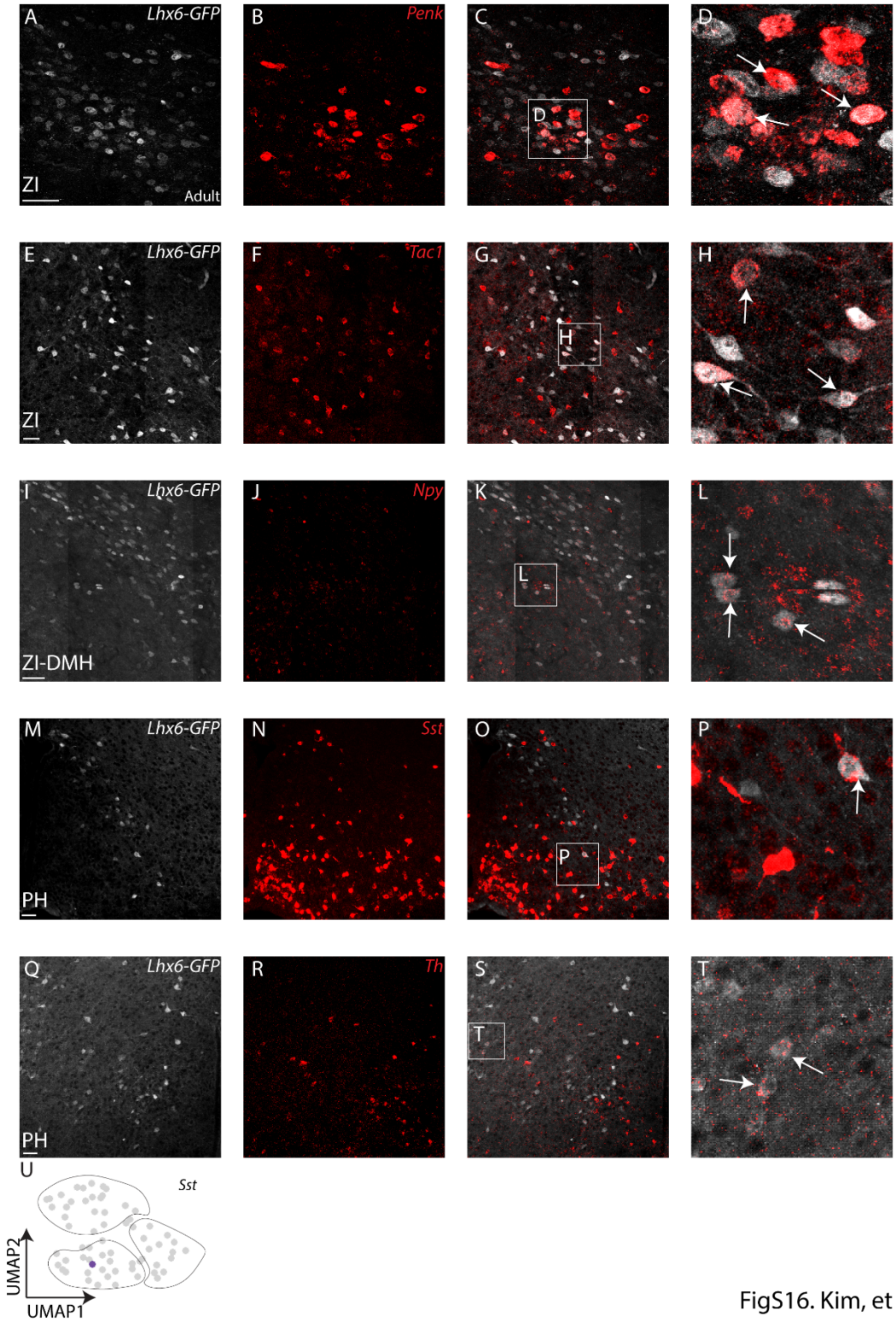

FigS16. Kim, et al.

Supplemental figure 16. Fluorescent *in situ* hybridization showing *Lhx6-GFP* (grey) with *Penk* (red, A-D), *Tac1* (red, E-H), *Npy* (red, I-L), *Sst* (red, M-P), and *Th* (red, Q-T). (U) UMAP plot showing *Sst* expression in ID or TT derived Lhx6^{+} neurons at P8. Scale bar = 50 µm.

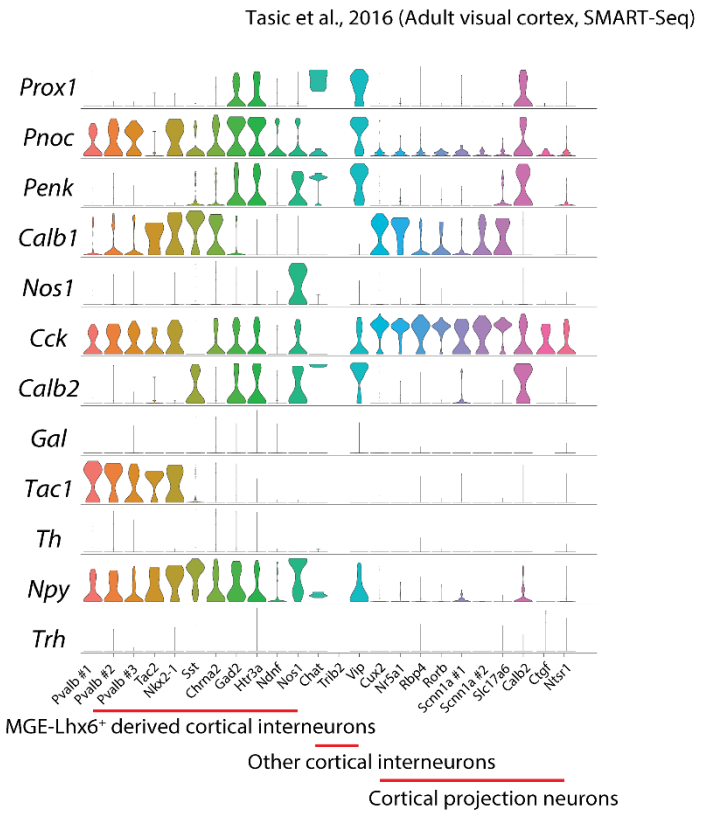

Supplemental figure 17. Violin plot gene expression of key neuropeptides and transmitters that are expressed in hypothalamic Lhx6^{+} cells in visual cortical neurons. Data from (Tasic et al., 2016).

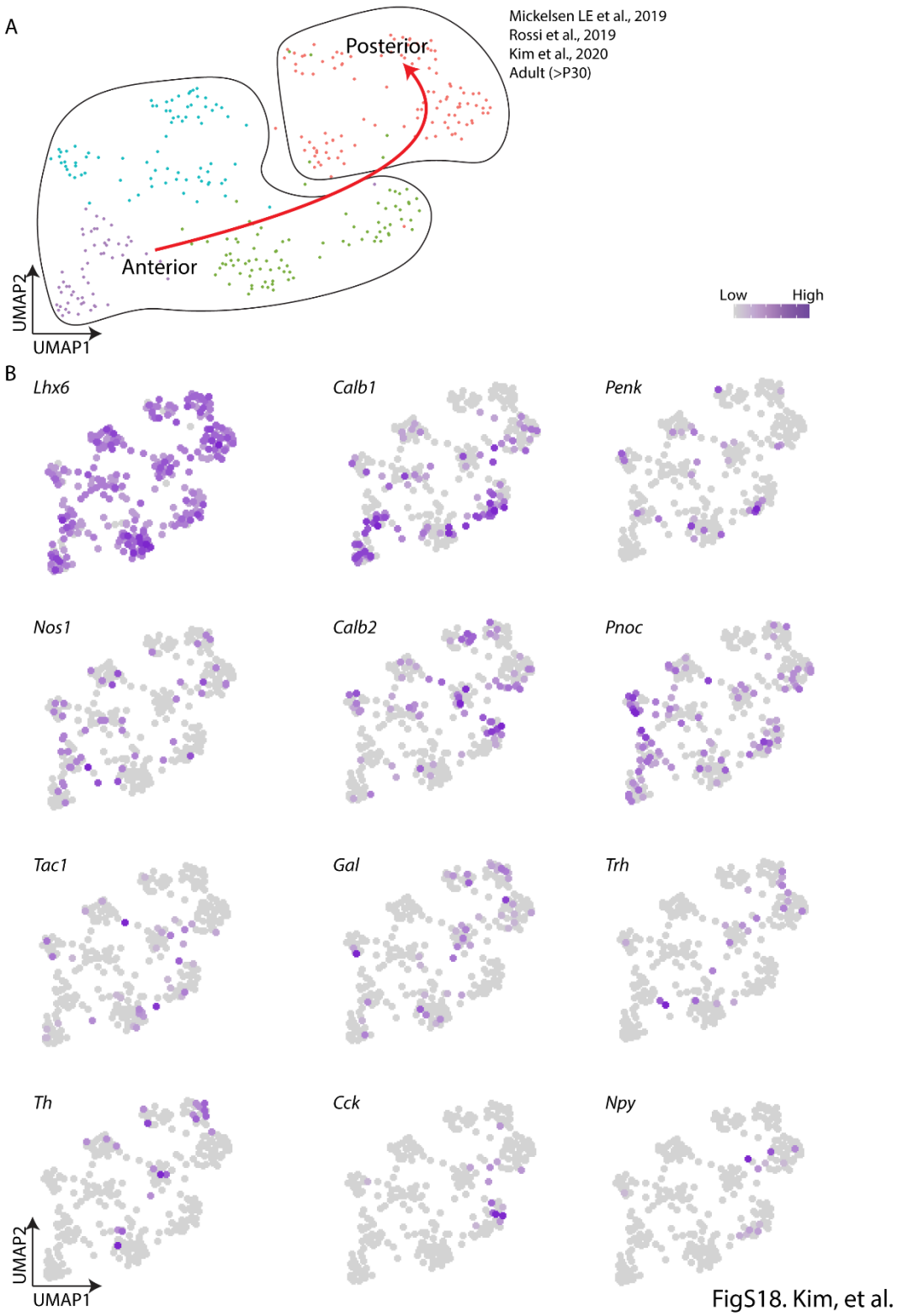

Supplemental figure 18. (A) UMAP plot showing Lhx6 neurons in adult (P30>) hypothalamus with anterior-posterior distribution. (B) UMAP plot showing expression of neuropeptide and neurotransmitters in adult Lhx6 neurons. Data from (D. W. Kim et al., 2019; Mickelsen et al., 2019; Rossi et al., 2019).

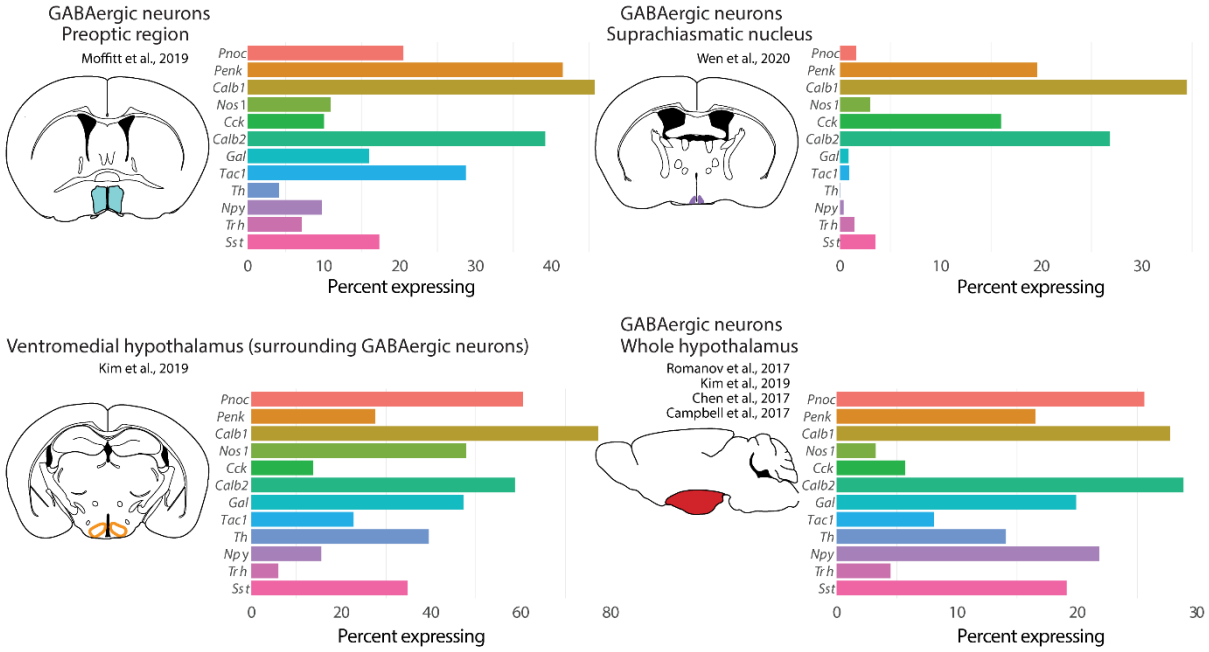

FigS19. Kim, et al.

Supplemental figure 19. Neuropeptides and neurotransmitters that are enriched in hypothalamic Lhx6^{+} neurons are widely expressed across GABAergic neurons of the hypothalamus - data from preoptic area (Moffitt et al., 2018), suprachasmatic nucleus (Moffitt et al., 2018; Wen et al., 2020), ventromedial hypothalamus (D.-W. Kim et al., 2019), and whole hypothalamus (Campbell et al., 2017; Chen et al., 2017; D. W. Kim et al., 2019; Romanov et al., 2017).

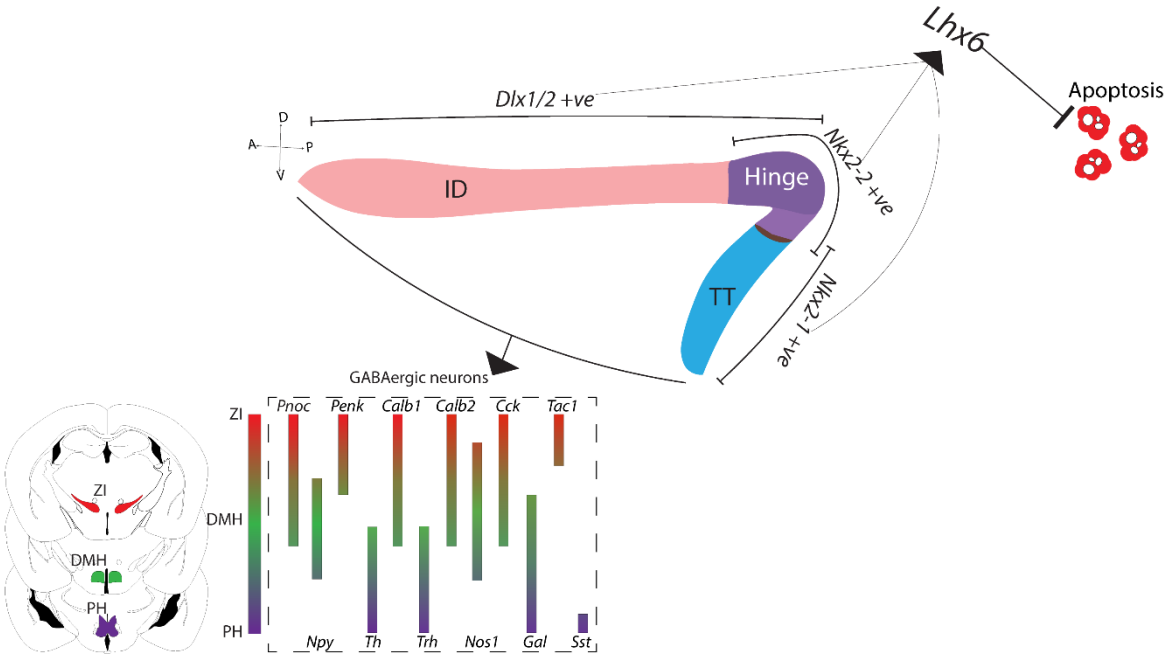

FigS20. Kim, et al.

Supplemental figure 20. Schematic summary of hypothalamic Lhx6 neurons

Table S6. Differential gene expression in E12.5 hypothalamic Lhx6 scRNA-Seq data.

Table S7. Differential gene expression in E13 MGE Lhx6 scRNA-Seq data. Data from (Mayer et al., 2018)

Table S8. Differential gene expression in E15.5 hypothalamic Lhx6 scRNA-Seq data.

Table S9. Differential gene expression in P8 hypothalamic Lhx6 scRNA-Seq data.

References:

Abecassis ZA, Berceau BL, Win PH, Garcia D, Xenias HS, Cui Q, Pamucku A, Cherian S, Hernández VM, Chon U, Lim BK, Justice NJ, Awatramani R, Kim Y, Hooks BM, Gerfen CR, Boca SM, Savio Chan C. n.d. Npas1 -Nkx2.1 Neurons Are an Integral Part of the Cortico-pallido-cortical Loop. doi:10.1101/644674

Amemiya HM, Kundaje A, Boyle AP. 2019. The ENCODE Blacklist: Identification of Problematic Regions of the Genome. *Sci Rep* **9**:9354.

Anderson SA, Qiu M, Bulfone A, Eisenstat DD, Meneses J, Pedersen R, Rubenstein JL. 1997. Mutations of the homeobox genes Dlx-1 and Dlx-2 disrupt the striatal subventricular zone and differentiation of late born striatal neurons. *Neuron* **19**:27–37.

Balderes DA, Magnuson MA, Sussel L. 2013. Nkx2.2:Cre knock-in mouse line: A novel tool for pancreas- and CNS-specific gene deletion. *genesis*. doi:10.1002/dvg.22715

Bartolini G, Sánchez-Alcañiz JA, Osório C, Valiente M, García-Frigola C, Marín O. 2017. Neuregulin 3 Mediates Cortical Plate Invasion and Laminar Allocation of GABAergic Interneurons. *Cell Rep* **18**:1157–1170.

Batista-Brito R, Rossignol E, Hjerling-Leffler J, Denaxa M, Wegner M, Lefebvre V, Pachnis V, Fishell G. 2009. The Cell-Intrinsic Requirement of Sox6 for Cortical Interneuron Development. *Neuron*. doi:10.1016/j.neuron.2009.08.005

Bedont JL, LeGates TA, Buhr E, Bathini A, Ling JP, Bell B, Wu MN, Wong PC, Van Gelder RN, Mongrain V, Hattar S, Blackshaw S. 2017. An LHX1-Regulated Transcriptional Network Controls Sleep/Wake Coupling and Thermal Resistance of the Central Circadian Clockworks. *Curr Biol* **27**:128–136.

Bedont JL, LeGates TA, Slat EA, Byerly MS, Wang H, Hu J, Rupp AC, Qian J, Wong GW, Herzog ED, Hattar S, Blackshaw S. 2014. Lhx1 controls terminal differentiation and circadian function of the suprachiasmatic nucleus. *Cell Rep* **7**:609–622.

Bedont JL, Newman EA, Blackshaw S. 2015. Patterning, specification, and differentiation in the developing hypothalamus. *Wiley Interdiscip Rev Dev Biol* **4**:445–468.

Bell BJ, Liu Q, Kim DW, Lee S, Liu Q, Blum I, Wang A, Bedont J, Chang A, Issa H, Cohen J, Blackshaw S, Wu MN. 2020. A Clock-Driven Neural Network Critical for Arousal. doi:10.1101/2020.03.12.989921

Buenrostro JD, Giresi PG, Zaba LC, Chang HY, Greenleaf WJ. 2014. Transposition of Native Chromatin for Fast and Sensitive Mulitmodal Analysis of Chromatin Architecture. *Biophysical Journal*. doi:10.1016/j.bpj.2013.11.503

Bulfone A, Puelles L, Porteus MH, Frohman MA, Martin GR, Rubenstein JL. 1993. Spatially restricted expression of Dlx-1, Dlx-2 (Tes-1), Gbx-2, and Wnt- 3 in the embryonic day 12.5 mouse forebrain defines potential transverse and longitudinal segmental boundaries. *The Journal of Neuroscience*. doi:10.1523/jneurosci.13-07-03155.1993

Campbell JN, Macosko EZ, Fenselau H, Pers TH, Lyubetskaya A, Tenen D, Goldman M, Verstegen AMJ, Resch JM, McCarroll SA, Rosen ED, Lowell BB, Tsai LT. 2017. A molecular census of arcuate hypothalamus and median eminence cell types. *Nat Neurosci* **20**:484–496.

Chen R, Wu X, Jiang L, Zhang Y. 2017. Single-Cell RNA-Seq Reveals Hypothalamic Cell Diversity. *Cell Rep* **18**:3227–3241.

Cobos I, Calcagnotto ME, Vilaythong AJ, Thwin MT, Noebels JL, Baraban SC,

Rubenstein JLR. 2005. Mice lacking Dlx1 show subtype-specific loss of interneurons, reduced inhibition and epilepsy. *Nat Neurosci* **8**:1059–1068.
Colasante G, Collombat P, Raimondi V, Bonanomi D, Ferrai C, Maira M, Yoshikawa K, Mansouri A, Valtorta F, Rubenstein JLR, Broccoli V. 2008. Arx is a direct target of Dlx2 and thereby contributes to the tangential migration of GABAergic interneurons. *J Neurosci* **28**:10674–10686.
Denaxa M, Kalaitzidou M, Garefalaki A, Achimastou A, Lasrado R, Maes T, Pachnis V. 2012. Maturation-promoting activity of SATB1 in MGE-derived cortical interneurons. *Cell Rep* **2**:1351–1362.
Denaxa M, Neves G, Rabinowitz A, Kemlo S, Liodis P, Burrone J, Pachnis V. 2018. Modulation of Apoptosis Controls Inhibitory Interneuron Number in the Cortex. *Cell Rep* **22**:1710–1721.
Dobin A, Davis CA, Schlesinger F, Drenkow J, Zaleski C, Jha S, Batut P, Chaisson M, Gingeras TR. 2013. STAR: ultrafast universal RNA-seq aligner. *Bioinformatics*. doi:10.1093/bioinformatics/bts635
Du T, Xu Q, Ocbina PJ, Anderson SA. 2008. NKX2.1 specifies cortical interneuron fate by activating Lhx6. *Development*. doi:10.1242/dev.015123
Erö C, Gewaltig M-O, Keller D, Markram H. 2018. A Cell Atlas for the Mouse Brain. *Front Neuroinform* **12**. doi:10.3389/fninf.2018.00084
Ewels P, Magnusson M, Lundin S, Käller M. 2016. MultiQC: summarize analysis results for multiple tools and samples in a single report. *Bioinformatics* **32**:3047–3048.
Flames N, Long JE, Garratt AN, Fischer TM, Gassmann M, Birchmeier C, Lai C, Rubenstein JLR, Marín O. 2004. Short- and Long-Range Attraction of Cortical GABAergic Interneurons by Neuregulin-1. *Neuron*. doi:10.1016/j.neuron.2004.09.028
Flandin P, Zhao Y, Vogt D, Jeong J, Long J, Potter G, Westphal H, Rubenstein JLR. 2011. Lhx6 and Lhx8 Coordinately Induce Neuronal Expression of Shh that Controls the Generation of Interneuron Progenitors. *Neuron*. doi:10.1016/j.neuron.2011.04.020
Fogarty M, Grist M, Gelman D, Marin O, Pachnis V, Kessaris N. 2007. Spatial Genetic Patterning of the Embryonic Neuroepithelium Generates GABAergic Interneuron Diversity in the Adult Cortex. *Journal of Neuroscience*. doi:10.1523/jneurosci.1629-07.2007
Gong S, Zheng C, Doughty ML, Losos K, Didkovsky N, Schambra UB, Nowak NJ, Joyner A, Leblanc G, Hatten ME, Heintz N. 2003. A gene expression atlas of the central nervous system based on bacterial artificial chromosomes. *Nature* **425**:917–925.
Hatori M, Gill S, Mure LS, Goulding M, O'Leary DDM, Panda S. 2014. Lhx1 maintains synchrony among circadian oscillator neurons of the SCN. *eLife*. doi:10.7554/elife.03357
Heinz S, Benner C, Spann N, Bertolino E, Lin YC, Laslo P, Cheng JX, Murre C, Singh H, Glass CK. 2010. Simple Combinations of Lineage-Determining Transcription Factors Prime cis-Regulatory Elements Required for Macrophage and B Cell Identities. *Molecular Cell*. doi:10.1016/j.molcel.2010.05.004
Huang ZJ, Paul A. 2019. The diversity of GABAergic neurons and neural communication elements. *Nat Rev Neurosci* **20**:563–572.
Humphreys BD, Lin S-L, Kobayashi A, Hudson TE, Nowlin BT, Bonventre JV, Todd Valerius M, McMahon AP, Duffield JS. 2010. Fate Tracing Reveals the Pericyte and Not Epithelial Origin of Myofibroblasts in Kidney Fibrosis. *The American*

Journal of Pathology. doi:10.2353/ajpath.2010.090517
Kessaris N, Magno L, Rubin AN, Oliveira MG. 2014. Genetic programs controlling cortical interneuron fate. *Current Opinion in Neurobiology*. doi:10.1016/j.conb.2013.12.012
Kim DW, Glendining KA, Grattan DR, Jasoni CL. 2016. Maternal Obesity in the Mouse Compromises the Blood-Brain Barrier in the Arcuate Nucleus of Offspring. *Endocrinology* **157**:2229–2242.
Kim DW, Washington PW, Wang ZQ, Lin SH, Sun C, Ismail BT, Wang H, Jiang L, Blackshaw S. 2019. The cellular and molecular landscape of hypothalamic patterning and differentiation. *bioRxiv*. doi:10.1101/657148
Kim D-W, Yao Z, Graybuck LT, Kim TK, Nguyen TN, Smith KA, Fong O, Yi L, Koulena N, Pierson N, Shah S, Lo L, Pool A-H, Oka Y, Pachter L, Cai L, Tasic B, Zeng H, Anderson DJ. 2019. Multimodal Analysis of Cell Types in a Hypothalamic Node Controlling Social Behavior. *Cell*. doi:10.1016/j.cell.2019.09.020
Kuleshov MV, Jones MR, Rouillard AD, Fernandez NF, Duan Q, Wang Z, Koplev S, Jenkins SL, Jagodnik KM, Lachmann A, McDermott MG, Monteiro CD, Gundersen GW, Ma'ayan A. 2016. Enrichr: a comprehensive gene set enrichment analysis web server 2016 update. *Nucleic Acids Research*. doi:10.1093/nar/gkw377
Langmead B, Salzberg SL. 2012. Fast gapped-read alignment with Bowtie 2. *Nat Methods* **9**:357–359.
Lein ES, Hawrylycz MJ, Ao N, Ayres M, Bensinger A, Bernard A, Boe AF, Boguski MS, Brockway KS, Byrnes EJ, Chen L, Chen L, Chen T-M, Chin MC, Chong J, Crook BE, Czaplinska A, Dang CN, Datta S, Dee NR, Desaki AL, Desta T, Diep E, Dolbeare TA, Donelan MJ, Dong H-W, Dougherty JG, Duncan BJ, Ebbert AJ, Eichele G, Estin LK, Faber C, Facer BA, Fields R, Fischer SR, Fliss TP, Frensley C, Gates SN, Glattfelder KJ, Halverson KR, Hart MR, Hohmann JG, Howell MP, Jeung DP, Johnson RA, Karr PT, Kawal R, Kidney JM, Knapik RH, Kuan CL, Lake JH, Laramee AR, Larsen KD, Lau C, Lemon TA, Liang AJ, Liu Y, Luong LT, Michaels J, Morgan JJ, Morgan RJ, Mortrud MT, Mosqueda NF, Ng LL, Ng R, Orta GJ, Overly CC, Pak TH, Parry SE, Pathak SD, Pearson OC, Puchalski RB, Riley ZL, Rockett HR, Rowland SA, Royall JJ, Ruiz MJ, Sarno NR, Schaffnit K, Shapovalova NV, Sivisay T, Slaughterbeck CR, Smith SC, Smith KA, Smith BI, Sodt AJ, Stewart NN, Stumpf K-R, Sunkin SM, Sutram M, Tam A, Teemer CD, Thaller C, Thompson CL, Varnam LR, Visel A, Whitlock RM, Wohnoutka PE, Wolkey CK, Wong VY, Wood M, Yaylaoglu MB, Young RC, Youngstrom BL, Yuan XF, Zhang B, Zwingman TA, Jones AR. 2007. Genome-wide atlas of gene expression in the adult mouse brain. *Nature* **445**:168–176.
Li B, Dewey CN. 2011. RSEM: accurate transcript quantification from RNA-Seq data with or without a reference genome. *BMC Bioinformatics*. doi:10.1186/1471-2105-12-323
Li H, Chou S-J, Hamasaki T, Perez-Garcia CG, O'Leary DDM. 2012. Neuregulin repellent signaling via ErbB4 restricts GABAergic interneurons to migratory paths from ganglionic eminence to cortical destinations. *Neural Dev* **7**:1–17.
Li H, Handsaker B, Wysoker A, Fennell T, Ruan J, Homer N, Marth G, Abecasis G, Durbin R, 1000 Genome Project Data Processing Subgroup. 2009. The Sequence Alignment/Map format and SAMtools. *Bioinformatics* **25**:2078–2079.
Lim L, Mi D, Llorca A, Marín O. 2018. Development and Functional Diversification of Cortical Interneurons. *Neuron* **100**:294–313.

Ling JP, Wilks C, Charles R, Leavey PJ, Ghosh D, Jiang L, Santiago CP, Pang B, Venkataraman A, Clark BS, Nellore A, Langmead B, Blackshaw S. 2020. ASCOT identifies key regulators of neuronal subtype-specific splicing. *Nat Commun* **11**:137.

Liodis P, Denaxa M, Grigoriou M, Akufo-Addo C, Yanagawa Y, Pachnis V. 2007. Lhx6 Activity Is Required for the Normal Migration and Specification of Cortical Interneuron Subtypes. *Journal of Neuroscience*. doi:10.1523/jneurosci.3055-06.2007

Liu K, Kim J, Kim DW, Zhang YS, Bao H, Denaxa M, Lim S-A, Kim E, Liu C, Wickersham IR, Pachnis V, Hattar S, Song J, Brown SP, Blackshaw S. 2017. Lhx6-positive GABA-releasing neurons of the zona incerta promote sleep. *Nature* **548**:582–587.

Madisen L, Zwingman TA, Sunkin SM, Oh SW, Zariwala HA, Gu H, Ng LL, Palmiter RD, Hawrylycz MJ, Jones AR, Lein ES, Zeng H. 2010. A robust and high-throughput Cre reporting and characterization system for the whole mouse brain. *Nat Neurosci* **13**:133–140.

Marín O, Baker J, Puelles L, Rubenstein JLR. 2002. Patterning of the basal telencephalon and hypothalamus is essential for guidance of cortical projections. *Development* **129**:761–773.

Maroof AM, Brown K, Shi SH, Studer L, Anderson SA. 2010. Prospective Isolation of Cortical Interneuron Precursors from Mouse Embryonic Stem Cells. *Journal of Neuroscience*. doi:10.1523/jneurosci.4255-09.2010

Martin M. 2011. Cutadapt removes adapter sequences from high-throughput sequencing reads. *EMBnet.journal*. doi:10.14806/ej.17.1.200

Mayer C, Hafemeister C, Bandler RC, Machold R, Batista Brito R, Jaglin X, Allaway K, Butler A, Fishell G, Satija R. 2018. Developmental diversification of cortical inhibitory interneurons. *Nature* **555**:457–462.

Mei L, Xiong W-C. 2008. Neuregulin 1 in neural development, synaptic plasticity and schizophrenia. *Nat Rev Neurosci* **9**:437–452.

Mickelsen LE, Bolisetty M, Chimileski BR, Fujita A, Beltrami EJ, Costanzo JT, Naparstek JR, Robson P, Jackson AC. 2019. Single-cell transcriptomic analysis of the lateral hypothalamic area reveals molecularly distinct populations of inhibitory and excitatory neurons. *Nat Neurosci* **22**:642–656.

Miranda-Angulo AL, Byerly MS, Mesa J, Wang H, Blackshaw S. 2014. Rax regulates hypothalamic tanycyte differentiation and barrier function in mice. *J Comp Neurol* **522**:876–899.

Moffitt JR, Bambah-Mukku D, Eichhorn SW, Vaughn E, Shekhar K, Perez JD, Rubinstein ND, Hao J, Regev A, Dulac C, Zhuang X. 2018. Molecular, spatial, and functional single-cell profiling of the hypothalamic preoptic region. *Science* **362**. doi:10.1126/science.aau5324

Newman EA, Wu D, Taketo MM, Zhang J, Blackshaw S. 2018. Canonical Wnt signaling regulates patterning, differentiation and nucleogenesis in mouse hypothalamus and prethalamus. *Dev Biol* **442**:236–248.

Piper J, Assi SA, Cauchy P, Ladroue C, Cockerill PN, Bonifer C, Ott S. 2015. Wellington-bootstrap: differential DNase-seq footprinting identifies cell-type determining transcription factors. *BMC Genomics* **16**:1000.

Pozas E, Ibáñez CF. 2005. GDNF and GFRalpha1 promote differentiation and tangential migration of cortical GABAergic neurons. *Neuron* **45**:701–713.

Qiu M, Bulfone A, Ghattas I, Meneses JJ, Christensen L, Sharpe PT, Presley R, Pedersen RA, Rubenstein JL. 1997. Role of the Dlx homeobox genes in

proximodistal patterning of the branchial arches: mutations of Dlx-1, Dlx-2, and Dlx-1 and -2 alter morphogenesis of proximal skeletal and soft tissue structures derived from the first and second arches. *Dev Biol* **185**:165–184.
Quinlan AR, Hall IM. 2010. BEDTools: a flexible suite of utilities for comparing genomic features. *Bioinformatics* **26**:841–842.
Robinson MD, McCarthy DJ, Smyth GK. 2010. edgeR: a Bioconductor package for differential expression analysis of digital gene expression data. *Bioinformatics* **26**:139–140.
Romanov RA, Zeisel A, Bakker J, Girach F, Hellysaz A, Tomer R, Alpár A, Mulder J, Clotman F, Keimpema E, Hsueh B, Crow AK, Martens H, Schwindling C, Calvigioni D, Bains JS, Máté Z, Szabó G, Yanagawa Y, Zhang M-D, Rendeiro A, Farlik M, Uhlén M, Wulff P, Bock C, Broberger C, Deisseroth K, Hökfelt T, Linnarsson S, Horvath TL, Harkany T. 2017. Molecular interrogation of hypothalamic organization reveals distinct dopamine neuronal subtypes. *Nat Neurosci* **20**:176–188.
Rossi MA, Basiri ML, McHenry JA, Kosyk O, Otis JM, van den Munkhof HE, Bryois J, Hübel C, Breen G, Guo W, Bulik CM, Sullivan PF, Stuber GD. 2019. Obesity remodels activity and transcriptional state of a lateral hypothalamic brake on feeding. *Science* **364**:1271–1274.
Ross-Innes CS, Stark R, Teschendorff AE, Holmes KA, Ali HR, Dunning MJ, Brown GD, Gojis O, Ellis IO, Green AR, Ali S, Chin S-F, Palmieri C, Caldas C, Carroll JS. 2012. Differential oestrogen receptor binding is associated with clinical outcome in breast cancer. *Nature* **481**:389–393.
Rueden CT, Schindelin J, Hiner MC, DeZonia BE, Walter AE, Arena ET, Eliceiri KW. 2017. ImageJ2: ImageJ for the next generation of scientific image data. *BMC Bioinformatics* **18**:529.
Salvatierra J, Lee DA, Zibetti C, Duran-Moreno M, Yoo S, Newman EA, Wang H, Bedont JL, de Melo J, Miranda-Angulo AL, Gil-Perotin S, Garcia-Verdugo JM, Blackshaw S. 2014. The LIM homeodomain factor Lhx2 is required for hypothalamic tanycyte specification and differentiation. *J Neurosci* **34**:16809–16820.
Sandberg M, Flandin P, Silberberg S, Su-Feher L, Price JD, Hu JS, Kim C, Visel A, Nord AS, Rubenstein JLR. 2016. Transcriptional Networks Controlled by NKX2-1 in the Development of Forebrain GABAergic Neurons. *Neuron* **91**:1260–1275.
Shimamura K, Hartigan DJ, Martinez S, Puelles L, Rubenstein JL. 1995. Longitudinal organization of the anterior neural plate and neural tube. *Development* **121**:3923–3933.
Shimogori T, Lee DA, Miranda-Angulo A, Yang Y, Wang H, Jiang L, Yoshida AC, Kataoka A, Mashiko H, Avetisyan M, Qi L, Qian J, Blackshaw S. 2010. A genomic atlas of mouse hypothalamic development. *Nat Neurosci* **13**:767–775.
Silbereis JC, Nobuta H, Tsai H-H, Heine VM, McKinsey GL, Meijer DH, Howard MA, Petryniak MA, Potter GB, Alberta JA, Baraban SC, Stiles CD, Rubenstein JLR, Rowitch DH. 2014. Olig1 function is required to repress dlx1/2 and interneuron production in Mammalian brain. *Neuron* **81**:574–587.
Stenman JM, Wang B, Campbell K. 2003. Tlx controls proliferation and patterning of lateral telencephalic progenitor domains. *J Neurosci* **23**:10568–10576.
Stuart T, Butler A, Hoffman P, Hafemeister C, Papalexi E, Mauck WM 3rd, Hao Y, Stoeckius M, Smibert P, Satija R. 2019. Comprehensive Integration of Single-Cell Data. *Cell* **177**:1888–1902.e21.
Takeuchi O, Fisher J, Suh H, Harada H, Malynn BA, Korsmeyer SJ. 2005. Essential

role of BAX,BAK in B cell homeostasis and prevention of autoimmune disease. *Proc Natl Acad Sci U S A* **102**:11272–11277.
Taniguchi H, He M, Wu P, Kim S, Paik R, Sugino K, Kvitsiani D, Fu Y, Lu J, Lin Y, Miyoshi G, Shima Y, Fishell G, Nelson SB, Huang ZJ. 2011. A resource of Cre driver lines for genetic targeting of GABAergic neurons in cerebral cortex. *Neuron* **71**:995–1013.
Tasic B, Menon V, Nguyen TN, Kim TK, Jarsky T, Yao Z, Levi B, Gray LT, Sorensen SA, Dolbeare T, Bertagnolli D, Goldy J, Shapovalova N, Parry S, Lee C, Smith K, Bernard A, Madisen L, Sunkin SM, Hawrylycz M, Koch C, Zeng H. 2016. Adult mouse cortical cell taxonomy revealed by single cell transcriptomics. *Nat Neurosci* **19**:335–346.
Vogt D, Hunt RF, Mandal S, Sandberg M, Silberberg SN, Nagasawa T, Yang Z, Baraban SC, Rubenstein JLR. 2014. Lhx6 directly regulates Arx and CXCR7 to determine cortical interneuron fate and laminar position. *Neuron* **82**:350–364.
Wang J, Zibetti C, Shang P, Sripathi SR, Zhang P, Cano M, Hoang T, Xia S, Ji H, Merbs SL, Zack DJ, Handa JT, Sinha D, Blackshaw S, Qian J. 2018. ATAC-Seq analysis reveals a widespread decrease of chromatin accessibility in age-related macular degeneration. *Nat Commun* **9**:1364.
Wang Y, Dye CA, Sohal V, Long JE, Estrada RC, Roztocil T, Lufkin T, Deisseroth K, Baraban SC, Rubenstein JLR. 2010. Dlx5 and Dlx6 Regulate the Development of Parvalbumin-Expressing Cortical Interneurons. *Journal of Neuroscience*. doi:10.1523/jneurosci.5963-09.2010
Watson C, Paxinos G. 2010. Chemoarchitectonic Atlas of the Mouse Brain. Academic Press.
Wen S ’ang, Ma D, Zhao M, Xie L, Wu Q, Gou L, Zhu C, Fan Y, Wang H, Yan J. 2020. Spatiotemporal single-cell analysis of gene expression in the mouse suprachiasmatic nucleus. *Nat Neurosci* **23**:456–467.
Wonders CP, Taylor L, Welagen J, Mbata IC, Xiang JZ, Anderson SA. 2008. A spatial bias for the origins of interneuron subgroups within the medial ganglionic eminence. *Dev Biol* **314**:127–136.
Yu G, Wang L-G, He Q-Y. 2015. ChIPseeker: an R/Bioconductor package for ChIP peak annotation, comparison and visualization. *Bioinformatics*. doi:10.1093/bioinformatics/btv145
Zhang Y, Liu T, Meyer CA, Eeckhoute J, Johnson DS, Bernstein BE, Nusbaum C, Myers RM, Brown M, Li W, Liu XS. 2008. Model-based analysis of ChIP-Seq (MACS). *Genome Biol* **9**:R137.
Zhao Y, Flandin P, Long JE, Cuesta MD, Westphal H, Rubenstein JLR. 2008. Distinct molecular pathways for development of telencephalic interneuron subtypes revealed through analysis of Lhx6 mutants. *J Comp Neurol* **510**:79–99.